

Applying Machine Learning Algorithms in the Design and Manufacturing Process of Bioinspired Architected Materials

Erfan Fatehi

Department of Bioresource Engineering

McGill University
Montréal, Québec
April 2021

A thesis submitted to McGill University in partial fulfillment of the requirement for the degree of Master of Science

©Erfan Fatehi, 2021

ACKNOWLEDGEMENTS

First and foremost, I would like to thank my supervisor, Prof. Abdolhamid Akbarzadeh at McGill University, and my co-supervisor, Dr. Behnam Ashrafi at the National Research Council of Canada (NRC-CNRC), for their kind and consistent support, incredible patience and guidance to help me in every step of the research.

I would like to also thank Dr. Hamidreza Yazdani, my friend and co-worker, for his insightful help, supervision and assistance.

I also would like to acknowledge the financial support from McGill University through graduate excellence, Ideation Funding National Research Council Canada, and McGill GPS funding through graduate internship program.

I would like to send my gratitude to my parents, whom I owe where I am today. Their warm-hearted and unlimited supports during my studies alongside my sibling Amir Nikan Fatehi was the greatest motivation I could ever ask for.

Finally, I thank my beloved friends, Alborz Karimi, Aidin Helal, Mahyar Jalali, Rasam Farasami, Mehrad Mortazavi, Athena Ardeshir and Nick Sagheb for their incredible emotional support and Hamed Niknam Jahromi, Alireza Kanani, Clement Beausoleil, Zach Katz and Ilhan Esmail for their technical support during my Master.

ABSTRACT

Precise material architectures and interfaces can generate attractive properties in materials. For example, Topologically Interlocked Materials (TIMs) are architectures that can turn brittle materials like ceramics into tough, deformable and impact-resistant material systems. This strategy has been adapted from biological materials such as nacre and tooth enamel, which have been in nature for millions of years. There are, however, some challenges in the mimicking of the biological materials and the production of TIMs. Designing TIMs for thermomechanical applications require in-depth thermomechanical finite element modelling (FEM). All possible architectures in the vast design space, containing many potential structures and configurations arranged in numerous ways, should be considered that is a computationally expensive process. This problem can be addressed by leveraging Machine learning algorithms that are mathematical models and a branch of artificial intelligence (AI).

This work consists of an extensive literature review on (1) bioinspired architected materials, especially topologically interlocked structures and (2) machine learning techniques and their applications in manufacturing, especially laser cutting of ceramic panels for the production of TIMs and (3) the designing of architected materials using ML algorithms. Later, in this study, we propose a new approach to design TIMs, using machine learning (ML), trained with finite element modeling (FEM) data and together with a self-learning algorithm, to discover high-performance ceramics in thermomechanical environments. First, a parametric study is conducted over topologically interlocked ceramic panels. A limited number of architectures is subjected to a thermal load and is studied using ANSYS finite element package. Finally, the multilinear perceptron is used to train the machine learning model on FEM data to predict the thermomechanical performance of architected panels (TIMs) with varied design parameters (e.g. interlocking angle and number of blocks).

Overall, the developed machine learning based framework can boost the design algorithm efficiency and provides new designs for various high-temperature applications in aerospace industries. This study demonstrates that architected ceramic panels with ML-assisted engineered patterns can demonstrate up to 30% improvement in frictional energy dissipation and 7% in the sliding distance of the tiles and 80% reduction in the strain energy that results in a higher safety factor and structural failure delay compared to plain ceramics subjected to a thermal load.

RÉSUMÉ

Des architectures et interfaces de matériaux précises peuvent générer des propriétés intéressantes dans les matériaux. Par exemple, les matériaux topologiquement imbriqués (TIM) sont des architectures qui peuvent transformer des matériaux fragiles comme la céramique en systèmes solides, déformables et résistants aux chocs. Cette stratégie s'inspire de matériaux biologiques tels que la nacre et l'émail dentaire qui sont utilisés avec succès dans la nature depuis des millions d'années. L'imitation de ces matériaux biologiques présente cependant de multiples défis : la conception de TIM pour des applications thermomécaniques nécessite une analyse par éléments finis (FEM) approfondie, et l'exploration de l'espace des configurations possible est coûteuse en calcul. Ce problème peut être résolu en tirant parti des algorithmes d'apprentissage automatique qui sont des modèles mathématiques et une branche de l'intelligence artificielle (IA).

Ce travail consiste donc en une vaste revue de la littérature sur (1) les matériaux architecturés bioinspirés, et notamment les structures topologiquement imbriqués, (2) les techniques d'apprentissage automatique et leurs applications dans la production, en particulier la découpe laser de panneaux céramiques pour la production de TIM ainsi que sur (3) la conception de matériaux architecturés à l'aide d'algorithmes ML. Plus tard, dans cette étude, nous proposons une nouvelle approche pour concevoir des TIM avec l'apprentissage automatique (ML), formés avec des données de modélisation par éléments finis (FEM) et avec un algorithme d'auto-apprentissage. Ceci afin de développer des céramiques haute performance dans des environnements sous contrainte thermomécaniques. Afin de mener ce projet à bien, une étude paramétrique est tout d'abord menée sur des panneaux céramiques imbriqués topologiquement. Un nombre limité d'architectures sont conçues, soumises à une charge thermique étudiée à l'aide des méthodes d'éléments finis ANSYS. Enfin, le perceptron multilinéaire est utilisé pour entraîner le modèle d'apprentissage automatique sur les données de FEM pour prédire les performances thermomécaniques des panneaux architecturés (TIM) avec des paramètres de conception variés (tel que l'angle de verrouillage et le nombre de blocs).

Dans l'ensemble, le cadre basé sur l'apprentissage automatique ainsi développé peut augmenter l'efficacité de l'algorithme de conception et fournir de nouvelles conceptions pour diverses applications à haute température dans les industries aérospatiales. Dans cette étude, il est démontré que les panneaux céramiques architecturés à motifs d'ingénierie conçus par ML montrent jusqu'à 30% d'amélioration de la dissipation d'énergie de frottement et 7% de la distance de glissement

des carreaux et une réduction de 80% de l'énergie de déformation. Ceci conduisant à un facteur de sécurité plus élevé et le délai de rupture structurelle par rapport aux céramiques simples soumises à une contrainte thermique.

Table of Contents

ACKNOWLEDGEMENTS	1
ABSTRACT	2
RÉSUMÉ	3
Prefaces and Contribution of Authors.....	7
Nomenclature	8
1 Introduction.....	9
1.1 Architected Materials.....	9
1.2 Machine Learning	11
1.3 Research objectives and goals of the thesis	11
2 Literature Review.....	12
2.1 Architected materials	12
2.2 Machine Learning Algorithms	18
2.2.1. What is Machine Learning?.....	18
2.2.2. Linear Regression	18
2.2.3. Neural Networks.....	20
2.2.4. Support Vector Machine Regression (SVR)	21
2.2.5. Decision Tree and Gradient Boosting	22
2.2.6. Machin Learning and Manufacturing.....	22
2.2.7. Smart machining:.....	23
2.2.8. Laser cutting:	23
2.3 Machine Learning and Architected Materials.....	30
2.4 Connecting Statement	31
3 Accelerated Design of Architected Ceramics with Tunable Thermal Resistance via Hybrid Machine Learning and Finite Element Approach.....	32
3.1 Introduction	33
3.2 Design Methodology	35
3.3 Finite Element Modeling.....	37
3.4 Machine Learning (ML).....	40
3.5 Results and Discussion.....	41
3.5.1. Architected Designs with Uniform Interlocking Angles.....	42
3.5.2. Exploring Designs with Variable Angles using Machine Learning	45

3.6 Concluding Remarks	53
3.7 Acknowledgments	55
3.8 Appendix	55
4 Summary, Discussion and Recommendation for Future Studies.....	58
4.1 Summary and Discussion	58
4.2 Recommendation for future studies	59
References.....	61

Prefaces and Contribution of Authors

This thesis has been written in a manuscript-based format and consists of a thorough literature review and one article submitted to a journal for publication.

The literature review in the first chapter was conducted and written by Erfan Fatehi and Prof. Akbarzadeh, Dr. Ashrafi and Dr. Yazdani reviewed and proofread.

Detailed contribution of the authors in the manuscript in **Chapter 3** is listed below:

Erfan Fatehi:

1. Conceptualization: Ideas; applying machine learning algorithms on the design optimization of interlocked architectures in thermomechanical applications.
2. Methodology: Development of hybrid ML-FEA algorithm.
3. Software: Programming and developing of ML algorithms, development of codes and conducting FEM.
4. Verification: Verification of ML results by conducting FEM analysis over the suggested designs from ML.
5. Data curation: Production of FEA data to feed ML algorithms and managing and processing the data.
6. Writing original draft: Preparation, creation and presentation of the research work, specifically writing the initial draft and applying comments and changes to the drafts of an article, prepared for submission to a journal.
7. Visualization: Preparation, creation and presentation of the manuscript. Visualization and presentation of the data.

Prof. Akbarzadeh, Dr. Ashrafi and Dr. Yazdani:

1. Review and editing: Providing a critical review, comments and revision in prepublication stages.
2. Supervision: Leading and giving oversight for the project.
3. Project administration: Managing and coordinating the research.

Nomenclature

Machine Learning	x	Input vector	y	Output vector
	ω	Weights	σ	Sigmoidal function
	ϕ_j	Base functions	h	Activation function
	μ	Average of input data	a	Activation
	s	Standard deviation	z	Hidden layer
Laser Machining	v	Linear speed (mm/s)	D_f	Focal position (mm)
	A	Amplitude (mm)	θ	Kerf taper of cut(angle $^\circ$)
	f_w	Wobble frequency (Hz)	D	Depth of cut(μm)
	N	Number of passes		
Manuscript	SF	Safety factor	E_{FDE}	Frictional dissipation energy
	σ_1 and σ_3	Maximum and minimum principal stresses	S_t	Tensile ultimate strength
	W_t	Mechanical energy	S_c	Compressive ultimate strength
	U	Internal energy	Q	Thermal energy
	E_{strain}	strain energy	W_{env}	Work on the environment

1 Introduction

1.1 Architected Materials

For decades mechanical and material engineers came together to find and produce materials with outstanding performances; however, they have suffered from significant mechanical and chemical trade-offs. For example, high strength in materials is at the expense of having low toughness [1] and high thermal stability at the expense of high density [2]. For instance, ceramics have great thermal performance and strength; however, controlling the brittleness of ceramics and manufacturing desired shapes out of ceramics are always a challenge that limits their usage in high-temperature applications.

Nature has always taught and provided human beings to survive and improve their life. As history advanced, natural materials such as bone and wood have slowly experienced an evolution. Scientists and engineers are amazed by the complex architectures of natural structures such as teeth, which can offer combinations of mechanical properties and surpass those of their constituent materials by orders of magnitude. This fascinating idea leads to the development of a new branch of advanced materials, i.e. bioinspired materials [3]. One example from nature is biomineralized ceramic tissues, which are particularly fascinating due to their remarkable mechanical resilience. Despite their brittle constituent building blocks, ceramic tissues have found ways to survive in harsh environments. A well-known example is nacre [4-7], in which plates of aragonite can boast far greater toughness than calcium carbonate individually. Aragonite tablets are combined with a soft material with lower Young's modules, helping them to become a tougher material. Another example is the skeleton of a sea sponge, which exhibits exceptional hierarchical levels of complexity, each providing the essential components of structural design necessary to convert the brittle constituent material (silica) into a sophisticated architecture [3]. This complex structure helps them to survive in a harsh environment. The tooth enamel also has unique characteristics. The enamel architecture has evolved to fulfill hard functions requiring cutting, crushing, and tearing of aliments. In humans, the enamel micro-architecture mainly consists of tightly packed (~96% vol.) hydroxyapatite rods. Hydroxyapatite is also constituent of bones in the human body and they are combined with proteins, making them the most mineralized and hardest material in the body [8]. Examples are shown in Figure 1.1 for different organisms and constituent materials. Superior mechanical performance of these structures has brought the idea of mimicking their

architectures in the form of architected materials. As opposed to the conventional materials, which gain their properties merely from their material composition, architected solids gain their extraordinary multifunctional properties mainly from their underlying architecture [9]. The next chapter will focus on human adaptations of interlocking structures, namely Topologically Interlocked Materials (TIMs).

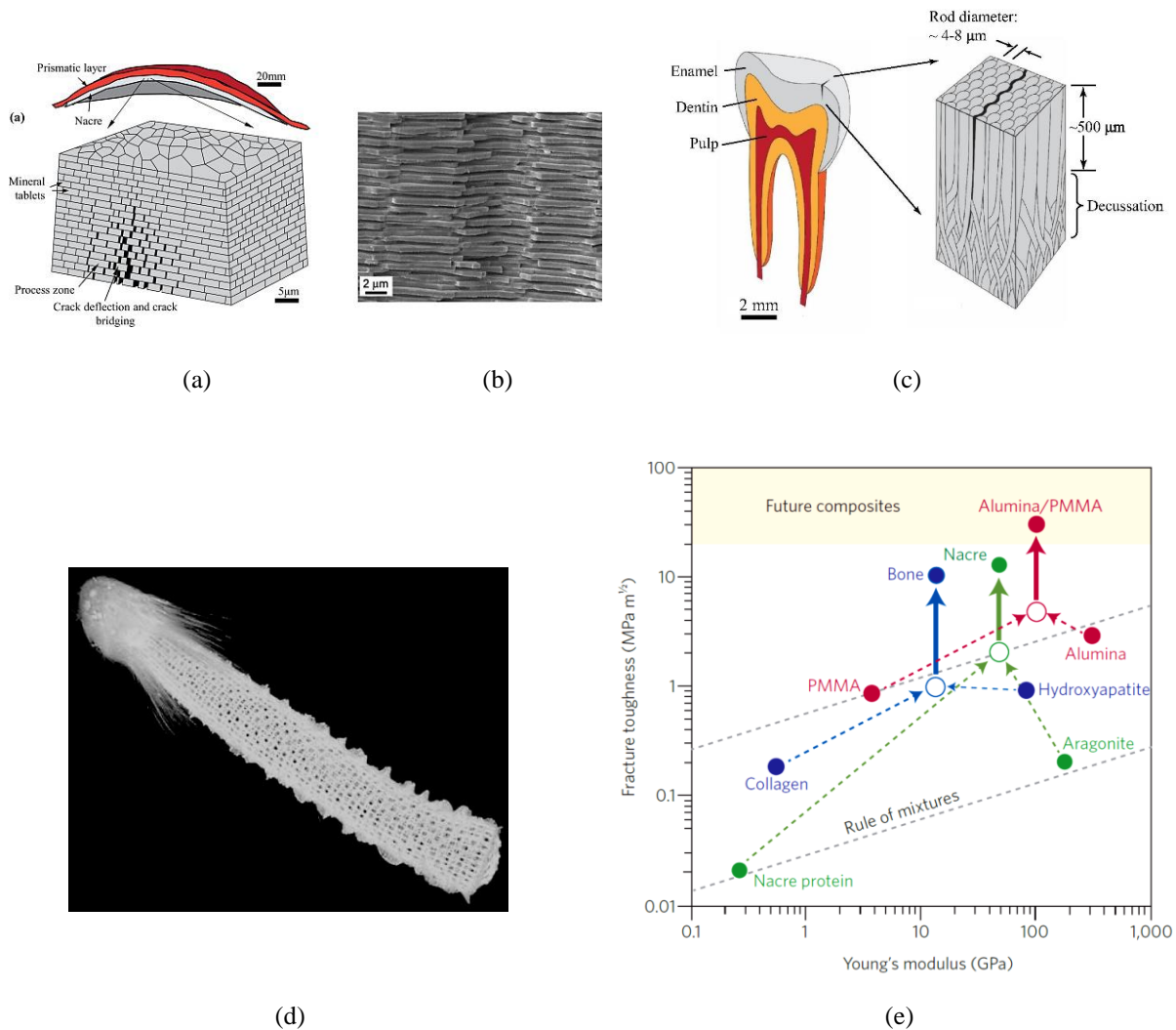


Figure 1.1: (a) Microarchitecture of nacre and the crack propagation [6]. (b) The fracture surface of the nacre showing the arrangement of tablets resulting in improving their toughness [7]. (c) The microstructure of tooth enamel [8]. (d) The glass sponge is showing the basket-like cage structure [10]. (e) The toughness of natural composite materials exceeding far from their constituents' toughness [11]. Reproduced with permission from the publisher.

1.2 Machine Learning

To this day, most of us have heard the word Artificial Intelligence (AI). No one can deny the importance of Artificial Intelligence in our daily life. When a person googles a topic, powerful algorithms are used to bring the most interesting results based on the previous search. Recommendation systems suggest items of interest and enjoyment to people based on their preferences. Machine learning (ML) algorithms is a branch of AI based on the idea that systems can learn from data, identify patterns and make decisions based on previous data. ML algorithms' usage is not limited to recommendation systems and can be expanded to other industries such as manufacturing and designing structures. As mentioned, bioinspired materials mimic the mechanical and biological characteristics of natural biomaterials from nature while difficult to design due to the complexity of their hierarchical and heterogeneous structures [3, 11-13]. The complexity of compositional and topological structures of bioinspired materials leads to vast design spaces that exceed the limit of available computers. It has been found that artificial intelligence (AI) and especially machine learning algorithms can address these problems. Numerous research articles in this topic are coming out in specific materials or mechanics branches, involving energy materials [14, 15], glasses [16], composites [17], polymers[18], bioinspired materials [19, 20], additive manufacturing, [13, 21-23]. Chapter 2 introduces several of the most important machine learning concepts, especially regression problems. Although some sophisticated machine learning algorithms might sound like daunting topics, they are in fact, straightforward and applicable in most engineering problems. Later we illustrate the usage of regression models in manufacturing, especially laser cutting. At the end of this work, machine learning techniques are used for investigating the thermomechanical performance of architected ceramics.

1.3 Research objectives and goals of the thesis

1. A thorough literature review over:
 - a) Bioinspired architected materials, especially topologically interlocked structures.
 - b) Machine Learning algorithms and their usage in manufacturing and design of architected materials.
2. Developing machine learning algorithms trained by FEM data and designing architected ceramics with tunable thermal resistance via the hybrid machine learning and FEM.

2 Literature Review

2.1 Architected materials

As we discussed in the introduction, architected Materials have brought us attractive characteristics and properties. For example, specific geometries can turn brittle materials such as ceramics into tough and impact-resistant materials. Many efforts have been made in improving the performance of materials, only focusing on their architectures [24]. High-performance structures that are stronger, tougher and lighter can be achievable by controlling structures at length scales that are intermediate between the microscale and the component's size. The mechanical properties, namely strength, wear resistance, stiffness, flexibility, fracture toughness and energy absorption, can be improved by having Fibrous, Helical, Gradient, Layered, Tubular, Cellular, Suture, Overlapping structures.

Fibrous structures are required for producing high tensile strength in a single direction. They are commonly found in soft biological materials, such as tendons [25] and silks [26]. These structures occur within the nano to microstructures of biological materials. Helical structures provide increased strength and toughness in multiple directions by employing layers with varying angles (twisted-ply structures).

Helically reinforcing structures are generally observed in the macrostructure of biological materials and organisms such as sea-sponge exoskeletons [27] and insect exoskeletons [28].

Gradient structures combine different materials with different mechanical properties, result in a structure gradient through their cross-section or thickness, such as fish scales [29] and crab claws [30].

Layered structures are employed to improve the toughness of brittle materials. the layers in these structures experience large changes in mechanical properties such as deep-sea sponges [31] and the brick and mortar structure of the abalone shell [32].

Tubular structures consist of arrays of long aligned pores within a bulk material such as horse hooves [33] and ram horns [34].

Highly porous structures, namely Cellular structures, are open and closed cell foams (e.g., honeycombs [35]), resulting in high-strength, low-weight structures, capable of resisting buckling and bending and increasing toughness, for instance, turtle shells [36] and bird bones [3].

Suture structures are wavy or interdigitating interfaces that are found within a variety of plates and bones and generally consist of two phases [37]: rigid suture teeth and a compliant interface layer to control the intrinsic strength and flexibility of a material interface. Suture structures are observed in armadillo osteoderms [38] and ammonite shells [39].

Overlapping structures, a group of structures consisting of TIMs, are structures composed of a number of individual plates or scales that can slide next to each other, forming a flexible protective surface such as seahorse tails [40] shark skin [41]. Mechanically interlocked structures are part of the group of overlapping structures that can ensure stiffness while allowing flexibility. The structures above are shown in Figure 2.1 [37].

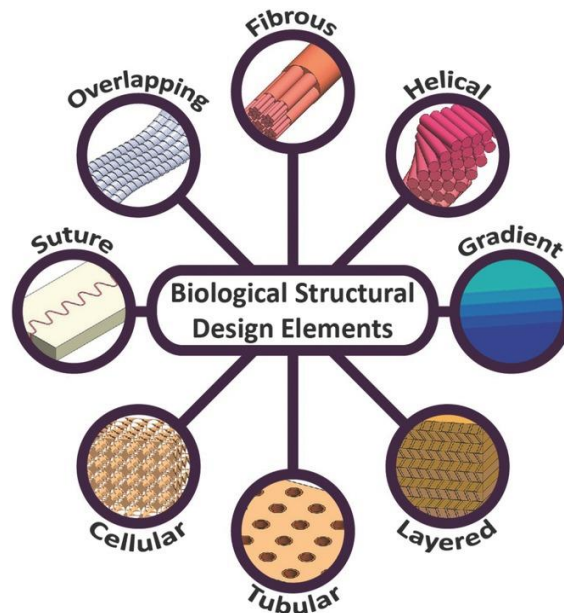


Figure 2.1: Diagram of the eight most common biological structural design elements [37]. Reproduced with permission from the publisher.

In this research, we mostly focus on Topologically Interlocking materials in brittle materials (also known as Masonry-type arrangement). These structures brought interesting characteristics such as localizing impact damage and increasing fracture toughness. By letting individual elements slide next to each other, high flexibility is achievable and applicable for a range of applications. In

TIMs, adjacent plates are locked within the structures without using any other materials such as adhesives and geometries are constrained by their peripheral supports.

Topologically Interlocked structures are mostly studied in impact applications [42]. TIMs localize the damage by hindering the crack propagation through the structure, where blocks in TIMs produce a solid structure by leveraging the friction between the tiles. The tough behavior of these structures is mostly due to the asperities on two rough surfaces. Different contact surfaces and designs of the blocks result in different interlocking architectures [43]. The idea of topological interlocking materials was motivated by the key block theory [44]. Some studies explored the mechanical performance of interlocking structures, especially the designs with tetrahedron tiles with mechanical testing [45].

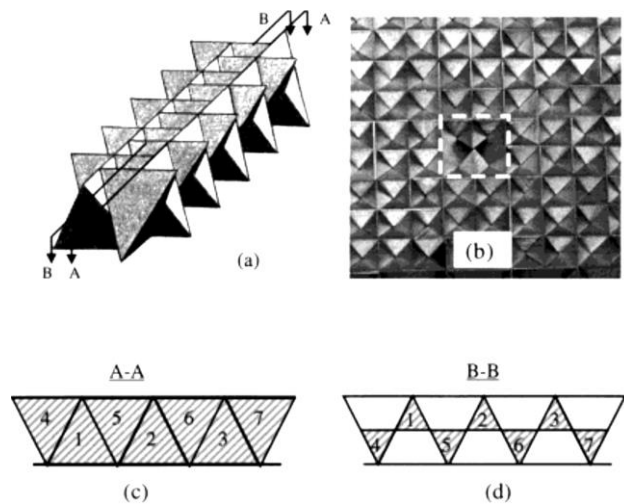


Figure 2.2: Topologically interlocked materials, tetrahedron design. (a) Schematic view of the adjacent tiles in the design. (b) Overview of whole structure with missing one tile. (c), (d) A-A and B-B cross-sections in the whole design [45]. Reproduced with permission from the publisher.

As well as mechanical testing, some mathematical models are established to capture the behavior of these architectures. It is beneficial to have a decent understanding of the mathematical models that inspire the development of codes and finite element analysis. According to experiments, indentation is one way to calculate the forces and out-of-plane deformations in TIMs. Khandelwal et al. tried to explore the mechanical properties of topologically interlocking material systems by applying indentation in the middle tile, which will cause different resultant forces on each cross-section plane [46]. Although results from experiments are more than 30% different from the analytical model, force-displacement trends are the same [47]. One of the drawbacks of

mathematical models is that they are limited to a certain boundary condition, and most of the time, it is not possible to be extended to other boundary conditions and loads and structures. The mathematical model of TIMs indentation is only valid for the same tetrahedron blocks, and it will be puzzling for analyzing structures containing different shapes of tetrahedron blocks. In Chapter 3, the FEM analysis is employed to calculate out-of-plane deformation and forces. Also, the randomness of different tetrahedrons with different angles is considered by leveraging machine learning (ML) models.

Some studies cover the usage of the other shapes of interlocking structures [43]. Also, the studies of TIMs are expanded by utilizing 3D printing and additive manufacturing methods [48], which give the ability to fabricate more complicated designs. Although 3D printing revolutionized the whole research area about bioinspired materials, there are still some challenges in printing all ranges of materials with desired porosity and strength, such as nonporous ceramics. Not only 3D printing, a variety of techniques such as Machining [49, 50], the casting of polyester [43] and cement paste [51] are used for the fabrication of TIMs. Some efforts have been made for manufacturing ceramic TIMs, for example, by freezing the gelation of ceramic slurries [52]. Ceramic panels produced by this way have more than 90% less compressive strength than nonporous ceramics, making them not favorable in harsh environments. Although nonporous ceramics have great performance, there are still many challenges in the manufacturing section. This study will discuss a laser cutting method to fabricate nonporous ceramics tiles in Topologically Interlocked structures.

In most of the studies, architected panels, especially TIMs, outperform the monolithic form of the material in terms of energy absorption, impact resistance and damage tolerance, but at the expense of flexural strength [43, 48, 50]. Architected panels display large and permanent deformations generated by the sliding and rotation of the tetrahedral blocks rather than by their materials' inherent characteristics. The force-deflection curve is shown (Figure 2.3) in 3D printed structure to demonstrate their behavior [24, 47]. Large deflection results in high energy absorption; this is observed in the area under the graph. Friction between the tiles plays a great role by dissipating energies and at the same time making the structure rigid [53]. These make TIMs attractive for impact-resistance applications [42, 50, 54, 55]. It is shown monolithic plain materials, which are made of brittle materials, fail catastrophically and can not absorb a higher amount of

energy. In contrast, interlocked architectures by localizing the damage could absorb higher energies till the whole structure collapse.

Another benefit of using TIMs is that some tiles remain intact and damaged tiles can be replaced [56]. In these materials, stiffness and toughness can be controlled by changing the design and arrangement of the tiles and still take advantage of other characteristics of brittle materials such as oxidation resistance, low thermal and electrical conductivity, refractory and most importantly, maintaining strength in high temperatures.

Many other shapes and contact surfaces can be designed and Finite Element Modelling assists us in exploring a limited number of designs [42, 47, 50, 53].

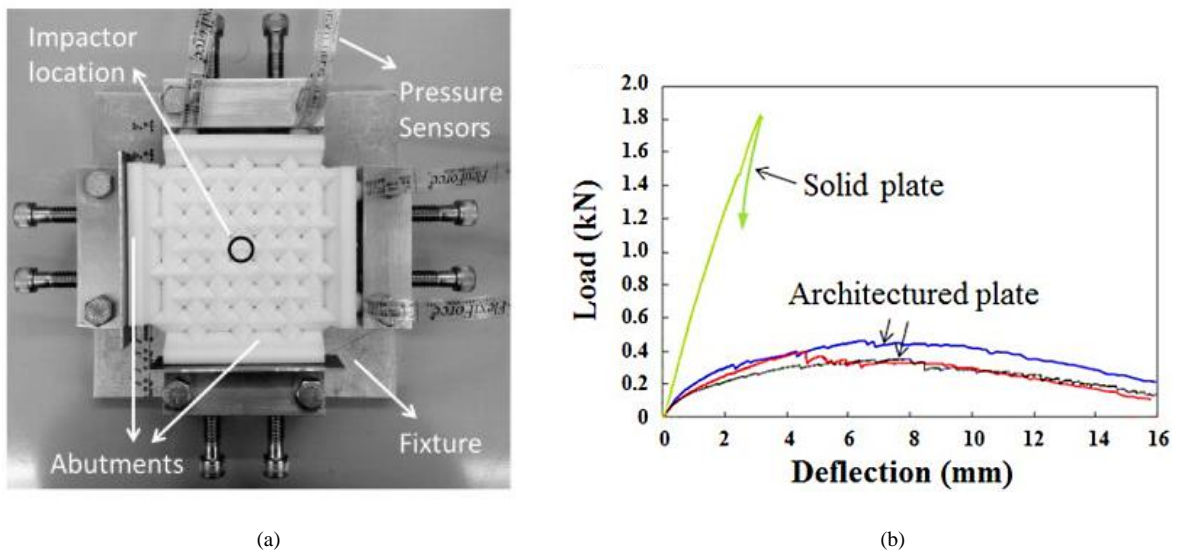
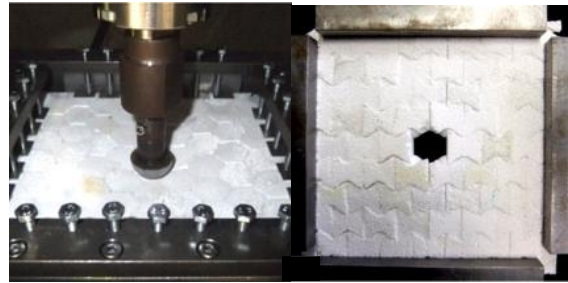


Figure 2.3: (a) 3D printed structure in impact test [47]. (b) Graph showing the tough behavior of interlocked architected materials [24]. Reproduced with permission from the publisher.

Despite the simplifications that the FEM models rely on, they can sometimes be accurate [47, 57, 58] and sometimes up to 14 times different from experiments [50]. Therefore experiments are needed for the validation of the results [57-59]. There are some limitations in the usage of FEM analysis; for example, FEM models are time-consuming. Recently new algorithms have been developed for increasing the speed of FEM models. Hybrid Machine learning and FEM algorithms are faster in time and beneficial to explore all possible designs. In the next section, we study different ML algorithms and we explore the usage of Machine Learning algorithms in mechanical engineering applications, especially architected materials design.



(a)



(b)

Figure 2.4: Comparison of catastrophic failure monolithic plate and localized damage in interlocked design. (a) Monolithic plain plate. (b) Topologically interlocked design [56]. Reproduced with permission from the publisher.

2.2 Machine Learning Algorithms

2.2.1. What is Machine Learning?

Machine learning is an application of artificial intelligence (AI) that provides systems the ability to observe and learn from existed data and predict the output for new input data. Most machine learning algorithms are divided into two problems which are regression and classification. In this chapter, after going through the definitions, we focus on the two most used regression algorithms, Logistic Regression and Neural Networks [60].

Regression and classification

In problems where training data is available and the model can be trained based on input vectors (instances) along with their corresponding target vectors, supervised learning algorithms are used. Cases such as image and digit recognition where the aim is to assign each input vector to one of a finite number of discrete categories are called classification. When the target vector (output) consists of continuous variables, the problem is called regression. An example of a regression problem would be predicting the depth of cuts in laser machining with specified input variables (we will elaborate on it in detail in this chapter).

2.2.2. Linear Regression

As we mentioned, Regression is supervised learning and its goal is to predict the value of one or more continuous target variables t given the value of a D -dimensional vector x of input variables. The polynomial fitting is an example of a broad class of functions called linear regression models. The simplest forms of linear regression models are linear fitting functions of the input variables. Besides linear and polynomial functions, we can obtain many more useful functions by taking linear combinations of a fixed set of nonlinear functions, known as basis functions. Given a training data set comprising N observations as instances and target values as outputs, the model will be trained based on the data. The goal of the model is to predict the value of output for new instance x .

From a probabilistic perspective, we aim to model the predictive distribution $p(t|x)$ because this expresses our uncertainty about the value of the predicted outputs for each value of x . Another goal is to minimize the expected value of a suitably chosen loss function from this conditional distribution. The loss function evaluates how well the algorithm models the dataset. The common

choice of loss function for real-valued variables is the squared loss. Linear regression, which is a linear combination of input variables, can be extended to different models by considering linear combinations of nonlinear functions of the input variables (basis functions) [60]:

$$y(x, w) = \omega_0 + \omega_1 x_1 + \dots + \omega_D x_D \quad (1.a)$$

$$y(x, w) = \sum_{j=0}^{M-1} \omega_j \phi_j(x) = w^T \phi(x) \quad (1.b)$$

Where x is known as the input vector and ω is known as the weights. ϕ_j is the base function. There are many possible options for base functions.

Polynomials, sigmoidal, Gaussians base functions in order are [60]:

$$\phi_j(x) = x^j \quad (2.a)$$

$$\phi_j(x) = \sigma\left(\frac{x-\mu_j}{s}\right), \quad \sigma(a) = \frac{1}{1+\exp(-a)} \quad (2.b)$$

$$\phi_j(x) = \exp\left\{-\frac{(x-\mu_j)^2}{2s^2}\right\} \quad (2.c)$$

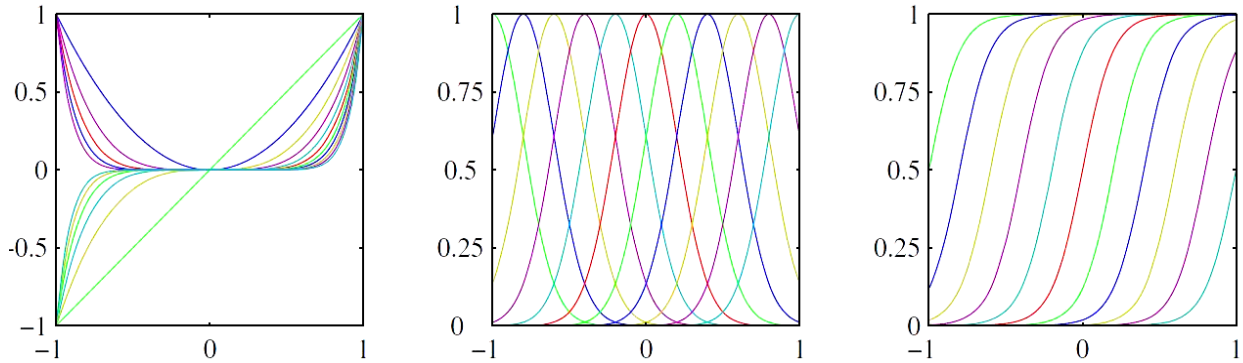


Figure 2.5: Comparison of Polynomials, sigmoidal, Gaussians base functions [60]

Weights of these basis functions are optimized by minimizing the loss function. The likelihood of the dataset is needed to be considered to interpret the probabilistic view of the functions. The likelihood function is a function for calculating the conditional probability of observing the data sample. The goal is to maximize the likelihood function that will result in minimizing the error function. Let us focus on linear basis functions and a probabilistic view of linear regression. Likelihood and log-likelihood and optimal weights are presented in order:

$$L(\omega) = \prod_{n=1}^N p_{\omega}(y^{(n)}|x^{(n)}) \quad (3.a)$$

$$l(\omega) = \sum_n -\frac{1}{2s^2} (y^{(n)} - \omega^T x^{(n)})^2 + \text{constant} \quad (3.b)$$

$$\omega^* = \operatorname{argmax}_\omega l(\omega) = \operatorname{argmin}_\omega \frac{1}{2} \sum_n (y^{(n)} - \omega^T x^{(n)})^2 \quad (3.c)$$

To find the minimum of the above function, the gradient of it is calculated and set to be zero. In this condition, a direct solution can be achieved however it is computationally expensive. For complex functions that direct solution is not applicable, methods such as gradient boosting are used to find the gradient of the functions [60]:

$$\omega^* = (X^T X)^{-1} X^T y \quad (4)$$

In this condition, nothing will be changed if we have nonlinear bases, $f_\omega = \sum_d \omega_d \phi_d(x)$ and the solution simply becomes: $\omega^* = (\Phi^T \Phi)^{-1} \Phi^T y$, where Φ is a matrix containing ϕ_d .

2.2.3. Neural Networks

Mathematical representations of information processing in biological systems [61] that can be used for pattern recognition in other applications called Neural Networks algorithms [62-65]. This section focuses on the specific class of neural networks that have proven to be of the greatest practical value, namely the multilayer perceptron [66, 67]. The goal is to extend the previous regression model by making the basis functions $\phi_d(x)$ depend on parameters and then to allow these parameters to be adjusted, along with the coefficients ω_j .

Neural networks use basis functions that are nonlinear functions of linear combinations of the inputs. A basic neural network model with two hidden layers is presented below [60].

$$a_j = \sum_{i=0}^D \omega_{ji}^{(1)} x_i, a_k = \sum_{j=0}^M \omega_{kj}^{(2)} z_j \quad (5.a)$$

$$y_k(X, w) = \sigma(\sum_{j=0}^M \omega_{kj}^{(2)} h(\sum_{i=0}^D \omega_{ji}^{(1)} x_i)) \quad (5.b)$$

In this formula $j = 0, \dots, M$ and $k = 0, \dots, K$ and superscript 1 and 2 indicate parameters in the first and second layers. Weights are presented by $\omega_{ji}^{(1)}$ and $\omega_{kj}^{(2)}$. a_j and a_k are known as activations. (a_j) In the first layer is transferred to the second layer using differentiable and nonlinear activation function h . There are a couple of choices for activation functions, namely, reLu, sigmoid and tanh. To find the network outputs y_k , output unit activations a_k are calculated. The output activations are then transformed using an appropriate activation function. For binary

classification problems, each output unit activation is transformed using a logistic sigmoid function (σ) [60, 68]. This idea can be extended to the models with more layers and a combination of different activation functions.

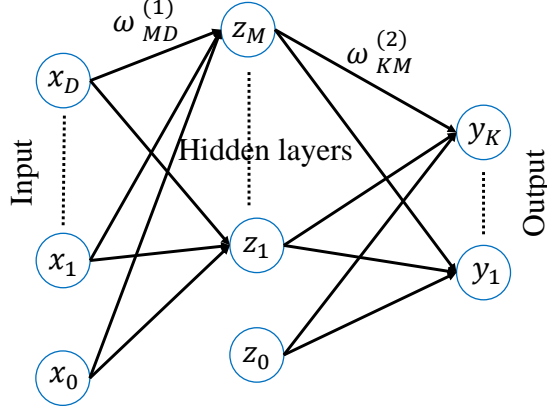


Figure 2.6: Schematic view of artificial neural networks with weights and activation functions.

In the next section, we demonstrate some applications of machine learning algorithms, especially regression algorithms, in manufacturing and designing.

2.2.4. Support Vector Machine Regression (SVR)

The SVR is the SVM implementation for regression and function approximation which has yielded good results in many regression problems in data mining [69]. The standard SVR formulation uses Vapnik's ϵ -insensitive cost function on the residuals $y_i - ((\Phi(x_i), \omega) + b)$ in such a way that errors up to ϵ are not penalized, and all further deviations will incur in a linear penalization. Briefly, SVR finds weights ω by minimizing the following regularized functional [70]:

$$\min_{\omega, \xi_i, b} \left\{ \frac{1}{2} |\omega|^2 + C \sum_i (\xi_i + \xi_i^*) \right\} \quad (6.a)$$

With respect to ω and to ξ_i^* (for $i = 1, \dots, n$), and constrained to:

$$y_i - ((\Phi(x_i), \omega) + b) \leq \epsilon + \xi_i, \quad \forall i = 1, \dots, n \quad (6.b)$$

$$((\Phi(x_i), \omega) + b) - y_i \leq \epsilon + \xi_i, \quad \forall i = 1, \dots, n \quad (6.c)$$

$$\xi_i, \xi_i^* \geq 0, \quad \forall i = 1, \dots, n \quad (6.d)$$

Where ξ_i^* are positive slack variables to deal with training samples with an absolute prediction error larger than ϵ ($\epsilon > 0$), and C is the penalization parameter applied to these ones. Note that C

trade-offs the minimization of errors and the regularization term, thus controlling the generalization capabilities.

2.2.5. Decision Tree and Gradient Boosting

A decision tree learner, a nonparametric supervised method, builds regression models in the form of a tree structure [71]. The goal is to predict the value of a target variable by learning simple decision rules inferred from the data features. Starting from the root (with the whole training data), data sets are broken down (split) at decision nodes into smaller and smaller subsets considering at each split the feature with maximal reduction of a weighted (with the number of samples) variability measure (e.g., mean square error). After a termination criterion is met, e.g., a prespecified maximum depth or maximum width is reached or, the result is a tree with decision and leaf nodes. A decision node has two (binary) branches, each associated with a set of values for the tested feature, while a leaf node represents a prediction (average value of the samples at the node) of the numerical target, i.e., function output.

GB as gradient boosting is designed to promote diversity among base learners in decision tree algorithm, hence reducing the covariance component of the generalization error and potentially improving prediction estimates, be robust to overfitting, which is the key factor to have better accuracies. As a by-product of the modeling process in gradient boosting algorithm, generate preliminary importance measures of the feature variables. We claim these objectives can be achieved by adopting a homogeneous ensemble approach based on decision trees and gradient boosting considering subsampling and random subspace strategies [72].

2.2.6. Machine Learning and Manufacturing

Every day unprecedented volume of data from experiments, simulations and measurements is produced in many fields such as engineering and manufacturing. Machine learning can act as a powerful tool to extract information from data and explain the pattern underlying the data. ML models also can augment new knowledge and automate different tasks that can assist in the understanding of models and optimization actions. This powerful framework can be beneficial in fields such as fluid mechanics [73, 74], where we should deal with massive amounts of data from experiments, field measurements, and large-scale numerical simulations. Over the past 50 years, Machine Learning techniques have been improved and extend their usage not only in applied science but also in industrial fields, such as manufacturing [75, 76].

Many different keys are playing a role in increasing the use of ML algorithms. Our generation is experiencing an unprecedented confluence of (a) vast volumes of data; (b) advances in the computer industry, (c) new efficient algorithms; (d) significant and ongoing investment by the industry on data-driven problem solving [77].

Recently scientific inquiry shifted from first principles to data-driven approaches as the models' accuracy needed to be increased and accomplish their goals. Since this thesis aims to focus on architected ceramic materials, in this section, we will explore the usage of Machine Learning algorithms in manufacturing ceramic panels using laser cutting. Later in Chapter 3, the usage of machine learning in exploring the behavior of architected materials.

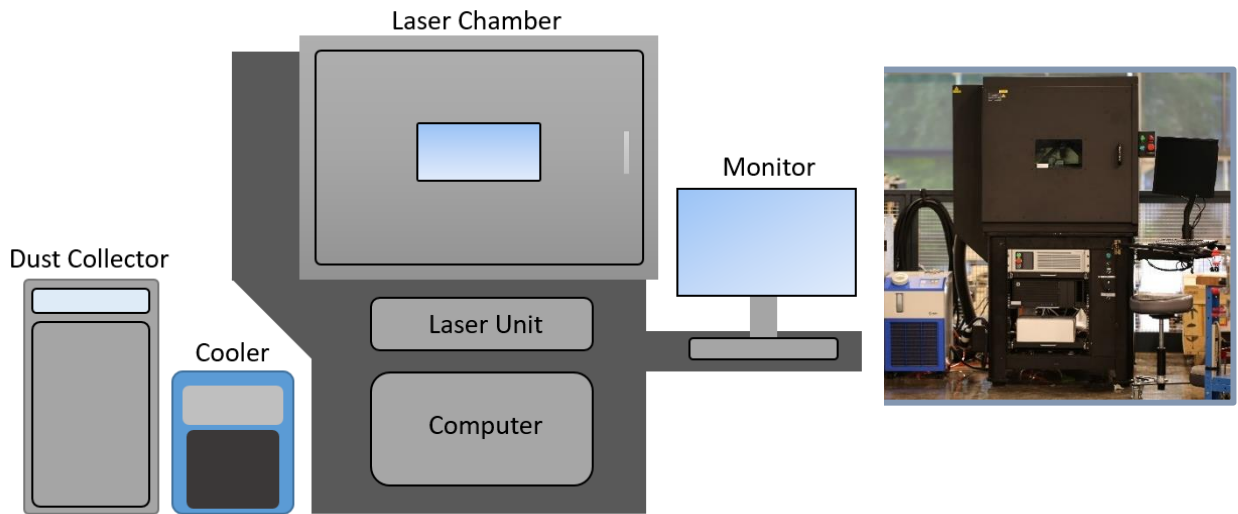
2.2.7. Smart machining:

Manufacturing sectors are now working on smart factories to improve productivity by processing the accumulated data using AI. There has been a steady increase in the demand for extracting information from large amounts of manufacturing data. Smart machining is a machining process that can adjust its parameters to achieve a certain objective. Some parameters are difficult to be tuned during conventional machining processes even by having the same operational condition. The smart machining process can be implemented to optimize process parameters and obtain optimum processing performance and product quality. There are various areas in machining that AI assists engineers, for example, milling for the purpose of tool wear monitoring [78-80], turning for the prediction of machine parameters [81] and abrasive waterjet for the prediction of surface roughness [82, 83]. This section mostly focuses on the laser cutting machine to produce deep ceramic cutting and Topologically Interlocked structures. We study machine learning algorithms' development for exploring the input parameters, which are amplitude, wobble frequency, linear speed, number of passes, and focal position to angle and depth of the cuts produced by the picosecond laser machine.

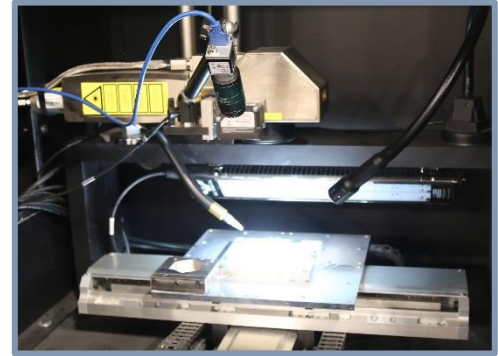
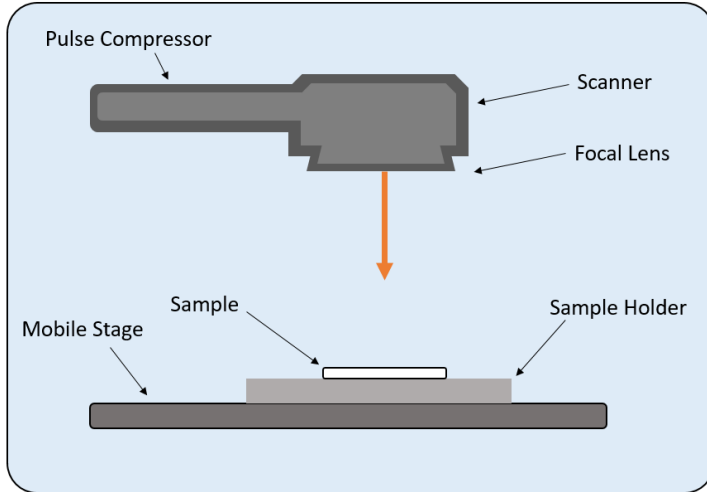
2.2.8. Laser cutting:

One of the main challenges with processing ceramics for interlocked structures is the machinability of ceramics for producing complex structures. Unlike metals, ceramics cannot maintain strength with traditional subtractive manufacturing techniques as the machined cuts are not damage-free [84]. Micro cracks produced as a result of machining of ceramics lead to crack initiation and finally, it can greatly reduce the strength of the ceramics [85-88]. With laser

processing, the material is no longer subject to vibration or cutting forces (shear forces) and instead is exposed to a high-energy beam, resulting in rapid ablation of the material. Ablation or sublimation is defined as the solid to gas phase transformation, bypassing the melting regime and liquid phase of the ceramic material. Characteristics of the surfaces and the properties of the work piece and the laser machine are important to the material removal during laser machining [89]. The interaction between surface and laser machining is influenced by controlling other machine-tool parameters such as pulse frequency, peak power, scanning speed and overlapping. Although many of these process parameters can be adjusted but still to obtain the desired quality and optimize the efficiency of the features being produced, we face many difficulties [90]. A few studies have been performed on the laser ablation of alumina ceramics [91-93] and some on systemically exploring the effects of the laser process parameters on high-quality cut geometries with a high degree of precision for alumina ceramics [94]. Ablation produced by laser cutting machine is utilized for manufacturing the interlocking ceramic panels. To have a better overview regarding the laser machine, Figure 2.7 illustrates the overall laser system located at the National Research Council of Canada (NRC-CNRC). The laser machine parts are broken down into Laser Chamber, Dust Collector, Cooler, Laser Unit (Ytterbium Picosecond Fibre Laser [YLPP-25-3-50-R, IPG Photonics, USA]), Computer and Monitor.



(a)



(b)

Figure 2.7: Schematic and realistic view of the laser system illustrating all the essential subsystems. (a) The laser machine system. (b) Laser chamber and its parts.

For the precise and deep cutting of ceramic samples, there are parameters to be tuned, such as the amplitude, wobble frequency, speed, number of passes and focal position. It is hard to control all of these parameters and there is a lack of knowledge about how different combinations of these parameters will affect the laser machining process. Various studies have investigated how laser process parameters independently affect the quality of the laser cuts. The influence of Amplitude, linear speed and the number of passes independently on cut quality and angle and depth of the cuts in alumina ceramics is studied in one of our previous works [91]. In another study, modifying pulse intensity, pulse frequency, pulse duration and air pressure resulting in a change in depth is studied [95]. Kumar and Gupta also investigated the influence of laser power, pulse frequency, number of scans and air pressure on the groove depth with a nanosecond pulsed fiber laser on stainless steel and aluminum [96].

Machine Learning (ML), a branch of AI, assists us in studying the effects of a different combination of parameters on the quality and depth of the cuts. ML is useful in the optimization and prediction of laser parameters. Karazi et al. investigated the effects of laser power, pulse frequency and scanning speed on the width and depth of the microchannels using artificial neural networks and compared ANN and DoE models to predict the width and depth of the channels [97]. Desai and Shaikh also predicted the depth of the cuts using ANN [98]. Also, other AI models such as Bayesian Networks are used to predict surface roughness [99]. In this section, the performance

and accuracies of different machine learning algorithms are investigated over 190 data points from experiments. The parameters that are studied in this section are presented in Table 2.1 with their definition and symbols.

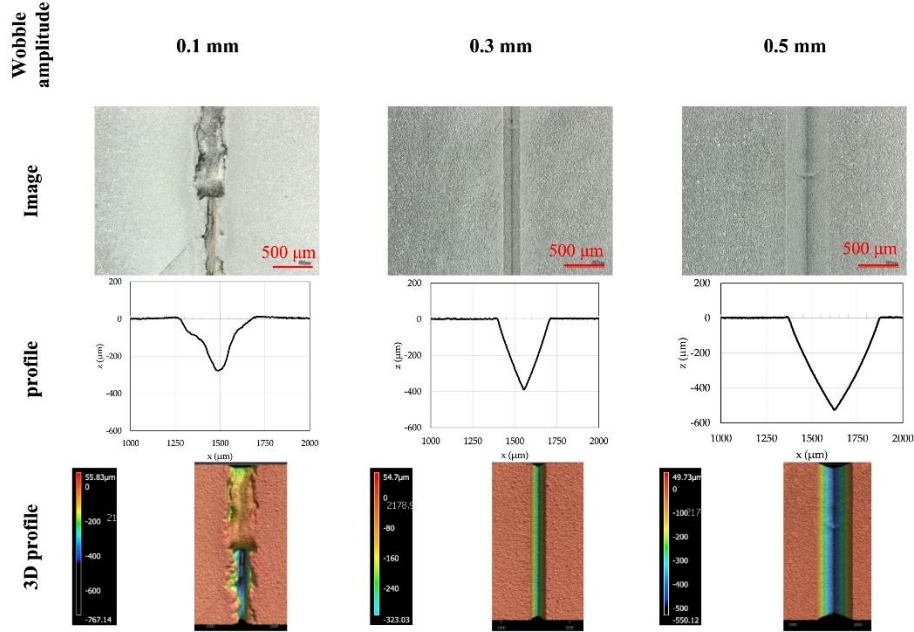


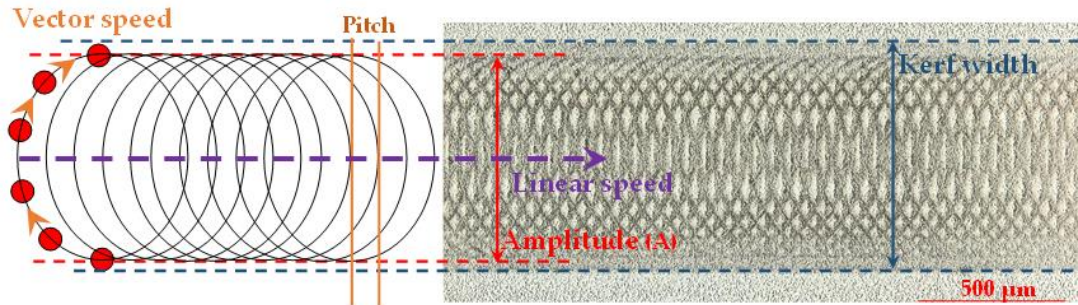
Figure 2.8: 3D laser scanning microscopy images and topography of ceramics for the linear speed of 20 mm/s with different wobble amplitude [91].

The correlation of input parameters which are amplitude, wobble frequency, linear speed, number of passes and focal position to angle and depth of the cuts, are investigated in the preprocessing step. Normalizing and scaling help the ML models converge and make the training less sensitive to features' scale. As shown in Figure 2.9, the correlation between the parameters indicates valuable information regarding the parameters. The number of passes and focal position has less impact on the angle of cuts than the amplitude, linear speed and wobble frequency. Focal position, number of passes and amplitude have less effect on the cuts' depth than linear speed and wobble frequency. In our previous works [91, 94], input parameters, the number of passes, linear speed, focal position, amplitude and wobble frequency are considered independent. However, the correlation between the parameters indicates that the linear speed and wobble frequency are highly correlated. Python and Matlab regression toolbox provide ML algorithms to explore different ML algorithms' accuracy (Linear regression, SVM, Tree, Gradient Boosting, Gaussian process regression and MLP) and to find the best performing algorithm. Multilayer perceptron (MLP), the

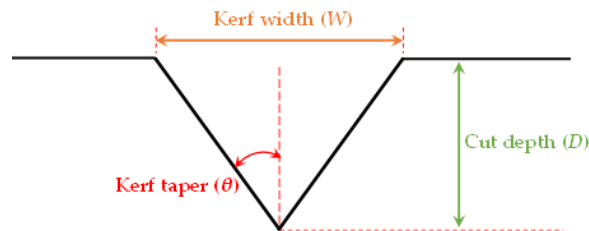
so-called feedforward artificial neural network for the regression problem (ANN) [60], shows lower Root Mean Square Error (RMSE) and higher R square values (Table 2.2) [100]. For this purpose, MLP regressor from the Sklearn library is used in Python. ReLu activation function has been used due to its higher accuracy than the logistic activation function. ReLu activation outputs directly the positive input and outputs the negative input to zero [101, 102]. Randomly, 10% of the dataset is picked for the test set and five-fold cross-validation is chosen to prevent overfitting. The mean accuracy of the MLP model reaches 85%, which shows the promising performance of the algorithm. Figure 2.10 true values and predicted values of depth and kerf taper are shown, which is another indication of the algorithm's performance.

Table 2.1: Laser input parameters with their symbols and definitions.

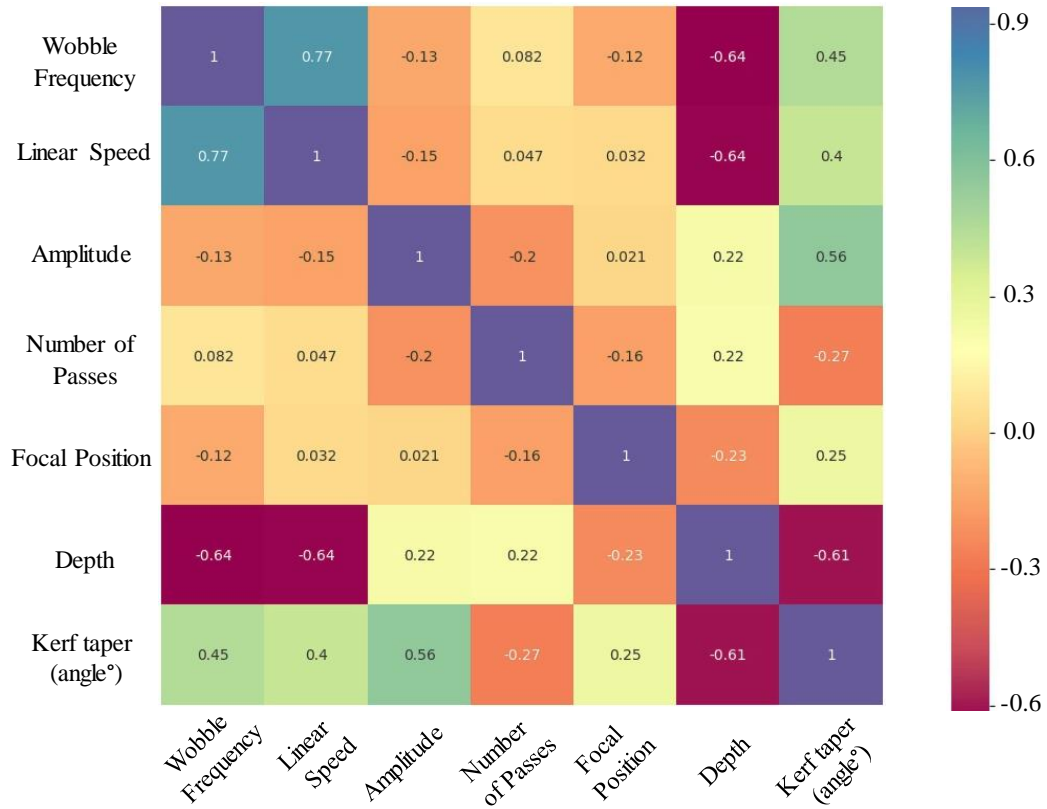
Parameter	Symbol	Description
Linear speed (mm/s)	v	The speed at which the tracking stage traverses
Amplitude (mm)	A	The diameter of the circles in the wobble
Wobble frequency (Hz)	f_w	Number of circular patterns per second
Number of passes	N	Number of times the laser scans a line
Focal position (mm)	D_f	The distance between the laser focus and the surface of the workpiece
Kerf taper (angle $^\circ$)	θ	The measured angle relative to the vertical axis
Depth (μm)	D	The measured depth of the cuts



(a)



(b)



(c)

Figure 2.9: (a) Presentation of input parameters [94]. (b) Presentation of output parameters of the laser machine [103]. (c) Correlation of input and output parameters of the laser machine.

Table 2.2: Comparison of ML algorithms with Root Mean Square Error and R-square Error. MLP has lower RMSE and higher R-square.

RMSE	Linear Regression	Tree	SVM	Gradient Boosting	Gaussian	MLP
Depth	90.08	80.11	50.17	86.03	41.34	36.73
Kerf taper	4.97	3.51	1.68	4.94	1.51	1.50

R-square	Linear Regression	Tree	SVM	Gradient Boosting	Gaussian	MLP
Depth	0.66	0.73	0.90	0.69	0.93	0.95
Kerf taper	0.72	0.86	0.97	0.72	0.97	0.97

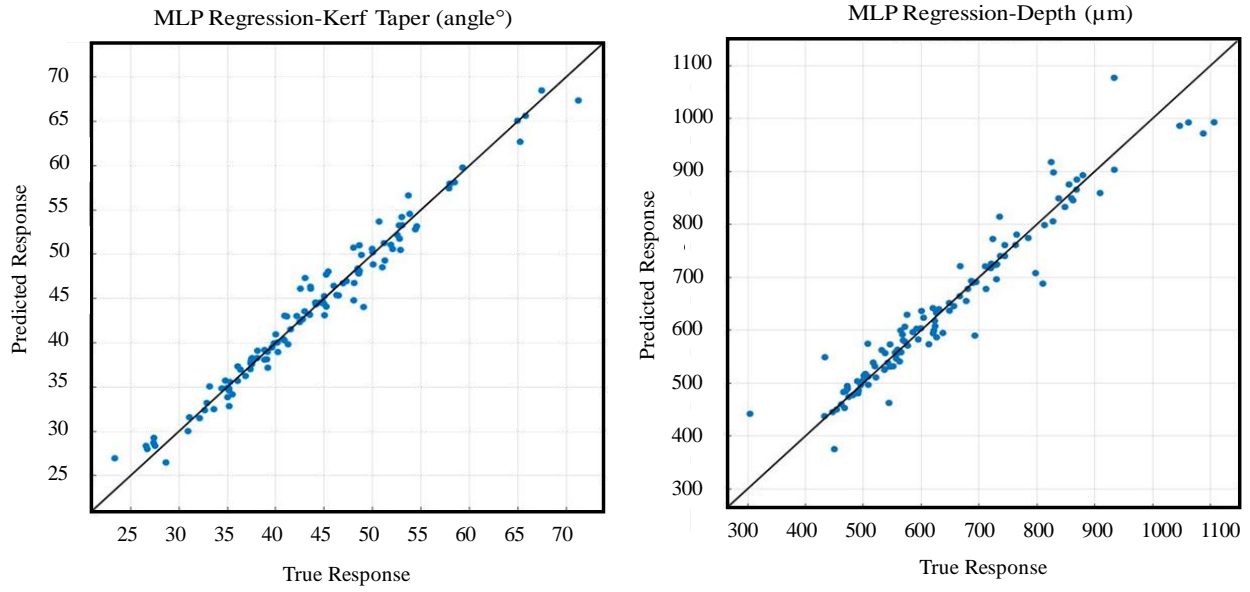


Figure 2.10: Presentation of the performance of MLP model by indicating the true and predicted responses.

For producing the interlocking ceramic samples, the trained machine learning algorithms play a great role in setting the laser machine's input parameters to specific values for the desired angle. In Figure 2.11, the laser machine cut the sample in two rounds and between the rounds, the ceramic sample is flipped and rotated. In Figure 2.11, 3×3, 5×5 and 7×7 interlocking ceramic samples are shown. At the end of Chapter 3 in the manuscript, we propose manufactured interlocking panels produced using the information mentioned above.

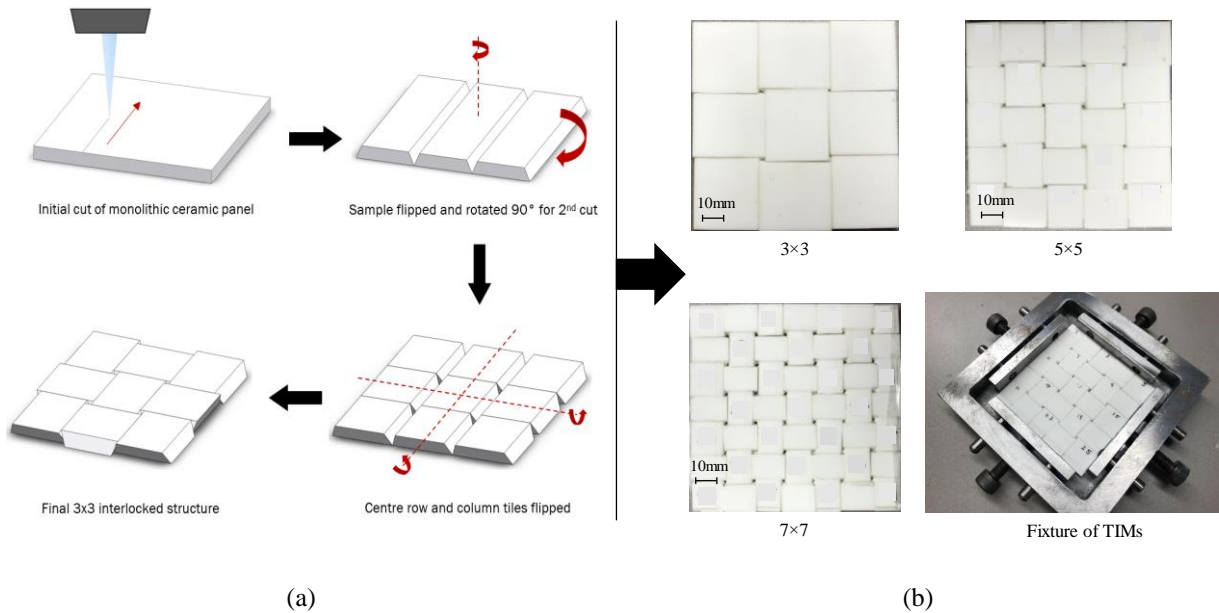


Figure 2.11: (a) Schematic of two round laser cutting for manufacturing of topologically interlocked panels. (b) 3×3, 5×5 and 7×7-block manufactured interlocked panels and the fixture for impact and thermal shock testing.

2.3 Machine Learning and Architected Materials

In previous sections, we explored the architected materials and machine learning algorithms separately. This section focuses on their combinations and reviews the growth and state of the art of new research efforts on architected materials design using ML.

Material engineering and mechanical engineering communities are aware of the great opportunities of leveraging ML as a powerful tool and a new paradigm. ML techniques have been utilized to search for new materials, exploring different material properties such as elasticity, plasticity, fatigue life, wear performance and buckling [13, 19, 104-108]. Some studies used ML in designing new materials with desired properties and validated results with different experimental techniques such as 3D printing of the newly designed architected materials [13, 23, 109]. Machine learning methods are used to develop design guidelines for biocomposites with high tensile strengths [110]. The production of data from FEM is efficient in terms of timing and cost compared to experiments. Integrated approaches combining finite element method and ML are developed to investigate the effect of constituent materials on composites' mechanical behavior [111]. MLP and convolutional neural networks demonstrated their capacity to accurately and efficiently predict the toughness and strength of two-dimensional (2D) composites [112] and it is possible to obtain the optimum structures of the composites in terms of strength and toughness. In another study, ANN predicted the unconfined compressive strength of cemented paste backfill [113]. ML models are employed to predict the compression strength of heat-treated woods [114]. Deep learning approaches were used for mining structure-property linkages in high contrast composites from simulation data sets [115, 116]. Deep learning models are also employed to capture nonlinear mapping between three-dimensional material microstructure and its macroscale stiffness [115].

2.4 Connecting Statement

Chapter 2 provided an extensive literature review on three important subjects to clarify the basics and help with the next chapter's comprehension.

- (a) Architected materials, especially topologically interlocked structures (TIMs)
- (b) Machine learning algorithms, especially regression models.
- (c) Employment of machine learning algorithms in manufacturing and Design of TIMs.

In Chapter 3, all subjects above are combined and are used to accelerate the design of topologically interlocked ceramic samples with tunable thermal resistance via hybrid machine learning and finite element approach.

3 Accelerated Design of Architected Ceramics with Tunable Thermal Resistance via Hybrid Machine Learning and Finite Element Approach

E. Fatehi^{1, 2}, H. Yazdani Sarvestani², B. Ashrafi^{2*}, A.H. Akbarzadeh^{1, 3*}

¹*Department of Bioresource Engineering, McGill University, Montreal, QC H3A0C3 Canada*

²*Aerospace Manufacturing Technology Center, National Research Council Canada, Montreal, QC H3T 2B2 Canada*

³*Department of Mechanical Engineering, McGill University, Montreal, QC H3A0C3 Canada*

Abstract

Ceramics have outstanding thermal performance; however, they are brittle that limits their applications in high-temperature environments. Designs such as topologically interlocked architectures can transform ceramics into tougher materials, while making the material design procedure a cumbersome task. One of the design challenges is to consider all feasible designs based on the topologically interlocked material strategy. Modeling the whole architectural design space is not efficient and to some degrees is not viable. In this study, we propose a new approach to design architected ceramics, using machine learning (ML), trained with finite element modelling (FEM) data and together with a self-learning algorithm, to discover high-performance ceramics in thermomechanical environments where inferior designs are phased out for candidates with superior properties. First, topologically interlocked panels are parametrically generated. Then, a limited number of designed architected ceramics subjected to a thermal load is studied using ANSYS finite element package. Finally, the multilinear perceptron is used to train the machine learning model using FEM data in order to predict the thermomechanical performance of architected panels with varied design parameters (e.g. interlocking angle and number of blocks). Overall, the developed machine learning based framework can boost the architected ceramic design efficiency and open new avenues for their functional controllability for various high-temperature applications in aerospace. This study demonstrates that the architected ceramic panels with ML-assisted engineered patterns show up to 30% improvement in frictional energy dissipation and 7% in the sliding distance of the tiles and 80% reduction in the strain energy, leading to a higher safety factor and the structural failure delay compared to plain ceramics subjected to a thermal load.

* Address correspondence to: A.H. Akbarzadeh (hamid.akbarzadeh@mcgill.ca, Tel: +1 (514) 398-7680) and B. Ashrafi (behnam.ashrafi@nrc-cnrc.gc.ca, Tel: +1 (514) 283-7421).

Keywords: *Architected ceramics; Interlocked building block; Machine learning; Finite element modeling; Thermal performance*

3.1 Introduction

Ceramics are used in a wide range of industrial sectors, including electronics [117], aerospace [118], medicine and biomedical devices [119-121], owing to their excellent properties such as oxidation resistance, low electrical conductivity, high refractory and maintaining their mechanical properties at high temperatures [122]. The low thermal conductivity of ceramics is used to protect space shuttles and keep satellites safe from serious damages [118], while their thermal stability property is critical in hypersonic flights and propulsion applications [123]. In spite of the excellent thermomechanical properties of ceramics, they generally suffer from brittleness [103, 122] that limits their multifunctional applications where ductility and toughness are required in addition to stiffness, strength and thermal resistance. Inspiration from natural and biological materials can assist to engineer the next generation of ceramics that can overcome the aforementioned drawback [124, 125].

Superior mechanical properties of biological species, such as a combination of high strength and high toughness, have inspired material scientists and engineers [126] to develop advanced high-performance materials [11]. In biological composites (e.g. bones, shells, horns and teeth), brittle organic materials such as calcium carbonate, calcium phosphate (hydroxyapatite), and amorphous silica [127] are employed by nature to design biomaterials that offer a combination of high strength, stiffness, flexibility, fracture toughness, and wear resistance [35, 128]. For example, the fracture toughness of abalone, conch shell and nacre with a brick and mortar microstructure [11, 129], is up to seven times higher than their material constituent, i.e., calcium carbonate [37]. Tooth enamel, as the hardest material in vertebrates, has also shown high toughness due to its microstructure that consists of tightly packed hydroxyapatite rods [3]. As a universal construction principle, these biological materials are made of hard and stiff building blocks bonded by weaker interfaces [130]. This finely-tuned strategy can result in deformation/failure mechanisms that enable the amplification of toughness. For example, the staggered architecture in nacre-like materials can result in progressive tablet sliding and crack blunting, deflecting, and bridging [131].

These microstructural designs have recently inspired the development of a new class of tough architected structures out of brittle materials such as ceramic and glass [55, 132].

One of the material design strategies to achieve superior mechanical performance is developing interlocked building blocks for architected materials that acts as a strain hardening mechanism to localize damages and spread the deformation to a larger volume of brittle materials [130]. The resulting materials are called topologically interlocked materials (TIMs) [133, 134]. Researchers have made considerable progress in the design and fabrication of TIMs to enhance their energy absorption and impact resistance capacity [50, 135-137]. Toughness has been improved in brittle materials by interlocked and segmented designs [50, 124]. The toughening mechanism is observed due to segmentation of blocks and the existence of weak interfaces (e.g. soft polymers such as ionomer or Ethylene-vinyl acetate (EVA) resins as an engineering replacement of protein in nacre) between microscale building blocks with tetrahedral, octahedral and cubic architectures [47, 53, 54, 57, 138]. These configurations offer a vast design space since the architectural features of the building blocks can be tailored by tuning their dimensions [57, 124] and interlocking angles [50, 54].

Machine Learning, a branch of artificial intelligence for discerning patterns from complex datasets, enables systems to learn from existing information in order to predict new results. ML algorithms have opened a great window to the horizon of all branches of science, such as diagnosis of diseases [139], discovering drugs [140] and image recognition [141]. Recently, ML algorithms have also found their applications to material selection and exploring new material properties [20, 105, 107, 108, 142-144]. While these studies demonstrate possible applications of using ML in materials design [142] (especially mechanical performance and architectures), they have been mainly focused on using ML models to predict the properties of materials rather than designing new structures with desired properties or functionalities.

Despite encouraging results of topologically interlocked panels in impact and energy absorption, more efforts are required to first evaluate and then optimize their performance in thermal applications. There are not sufficient studies on the thermal behavior of bioinspired brittle materials and specifically ceramics. In this study, the thermal performance of architected ceramics with topologically interlocked designs is studied and a new approach is introduced to design architected ceramics using a combination of FEM and ML (Figure 3.1). Here a database of 400 panels from finite element analysis is used to train a model for discovering high-

performance ceramic panels. This hybrid ML-FEM model is computationally efficient for evaluating the thermal and mechanical performance of the designed architected ceramics. The dissipation energy through friction between blocks, energy absorption and architectural failure based on safety factor are explored using finite element analysis to find high-performance architectural designs. Neural Networks are used to explore the performance of 400,000 topologically interlocked designs with distinct dimensions and interfacial angles between neighboring blocks. At the end, the designs are analyzed by FEM to explore the accuracy of predictions. In Figure 3.1, the schematic of the design algorithm is presented: (Step 1) Architected panels are designed and design parameters are set using a CAD software package; (Step 2) Architected designs with specific dimensions are produced; (Step 3) Boundary conditions and external thermal load are applied on the panels; (Step 4) Performance of alternative designs are explored by specifying the output parameters (e.g. deflection, energies, reaction forces and safety factor); and (Step 5) ML algorithms are trained by all results from the previous procedure in order to select better performing architectural designs.

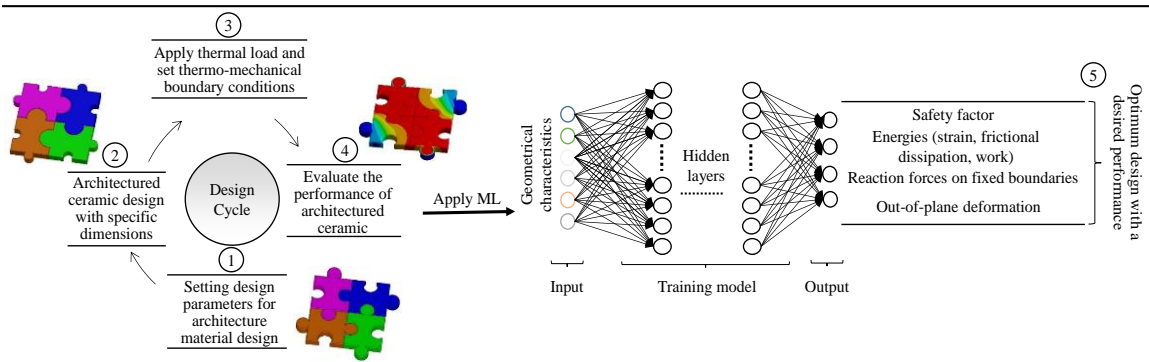


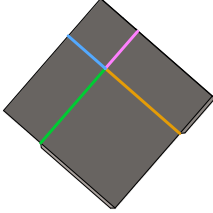
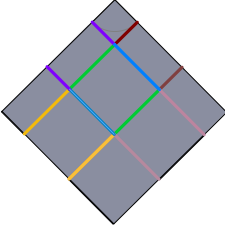
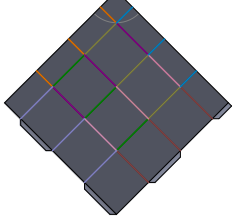
Figure 3.1: Schematic of the design algorithm for finding the best performing architecture with respect to the desired output (e.g. safety factor, energies (strain, frictional dissipation, work), and reaction forces). Jigsaw panels are used to represent an example of architected materials.

3.2 Design Methodology

Topologically interlocked panels [50] are built from truncated non-platonic tetrahedron ceramic blocks (see Figure 3.2a). The blocks with an interlocking angle (α and β) less than 90° are contained by adjacent blocks, resulting in a topologically interlocked design. A non-regular truncated tetrahedron has two planar surfaces: a square on the bottom and a rectangle on the top (Figure 3.2a). A non-regular tetrahedron is truncated unsymmetrically from top and bottom to ensure a square area with $l \times l$ dimensions on one side of truncated tetrahedron is produced. Angles

on sides AA and BB may be different (α and β in Figure 3.2b). For each block two faces are tilted outward, and the other two are tilted inward. The height of the building block is set to be $h = 2.54 \text{ mm}$ (0.1 inch) and dimensions of the rectangular section is $l + 2h \times \tan(\alpha)$ and $l - 2h \times \tan(\beta)$. The panels with different numbers of blocks, including 3×3 , 5×5 and 7×7 , are considered. The overall size of the 3×3 , 5×5 and 7×7 panels is set to be $10 \times 10 \text{ cm}^2$. Considering two symmetry planes, the panels have 4, 6 and 8 possibilities of different interlocking angles for the 3×3 , 5×5 and 7×7 structures, as reported in Table 3.1, respectively. Interlocking angles studied here are 5° , 10° , 15° , 20° and 25° that result in 625, 15625 and 390625 combinations for 3×3 , 5×5 and 7×7 panels, correspondingly. Three-dimensional displacements and rotations on all four boundaries of the panels are constrained to make fully interlocked geometries. These panels are fully constrained without using any other materials between the tiles, like adhesive. A thermal load applied to the center of the architected panel generates transverse mechanical forces and frictional interactions between blocks. The panel also experiences an out-of-plane deformation that is distinct from the pristine ceramic panel as a baseline for comparing the thermomechanical behaviors.

Table 3.1. All possible architected designs by changing the angles between blocks. Each color represents an angle (α, β).

Number of blocks	Interlocking angles (α, β)	Number of designs with alternative interlocking angles	Arrangement
3×3	$5^\circ, 10^\circ, 15^\circ, 20^\circ, 25^\circ$	$5^4 = 625$	
5×5	$5^\circ, 10^\circ, 15^\circ, 20^\circ, 25^\circ$	$5^6 = 15625$	
7×7	$5^\circ, 10^\circ, 15^\circ, 20^\circ, 25^\circ$	$5^8 = 390625$	

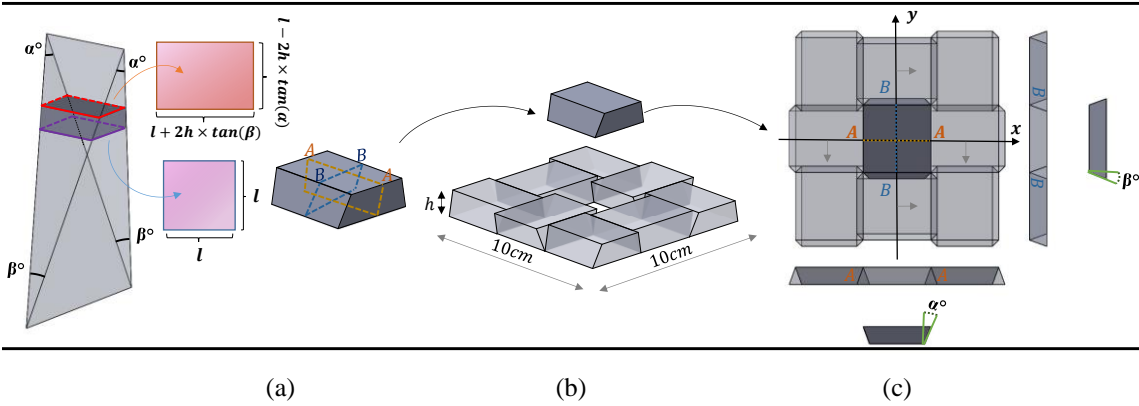


Figure 3.2: Overview of the design of the topologically interlocked panel. (a) Truncated non-regular tetrahedron. (b) Block with different angles in AA and BB surfaces and the locking configuration of adjacent blocks in the 3×3 block panels. (c) Symmetry planes in the architecture panel and different angles of blocks on each side (α, β).

3.3 Finite Element Modeling

FEM is performed using ANSYS Workbench 2019 R3 on panels with different numbers of building blocks and interlocking angles. Panels with the 3×3 (9), 5×5 (25) and 7×7 (49) arrays of blocks as well as 5° , 10° , 15° , 20° and 25° interlocking angles are considered. The architected designs have two symmetry planes, one normal to the x -direction and one normal to the y -direction (see Figure 3.2c). Material properties of non-porous alumina ceramics are assumed to be isotropic linear elastic. Different properties of the alumina ceramics are listed in Table 3.2 [124]. These properties are considered constant in the range of temperature analysis. Transient thermal analysis is first performed to evaluate the thermal performance of different architected designs. A constant temperature (i.e., thermal load) is applied to a circular area with a radius of 10 mm in the middle of the panel. The rest of the panel containing edges is exposed to free convection with a heat transfer coefficient of $10 \frac{W}{m^2K}$. Due to the fixed boundaries in peripheral blocks, the thermal expansion of the panel results in in-plane forces between building blocks. A thermomechanical study is performed to explore the mechanical behavior of the panels under the thermal load. Coulomb-Mohr failure criterion (see Eq. 3.1) for brittle materials is employed to evaluate the safety factor (SF) of each design, which is the minimum of the safety factor of all material points in the architected ceramic [145]:

$$SF = \min \left(\begin{cases} \frac{S_t}{\sigma_1} & \sigma_1 \geq \sigma_3 \geq 0 \\ \frac{S_t}{\sigma_1 - \frac{S_t}{S_c} \sigma_3} & \sigma_1 \geq 0 \geq \sigma_3 \\ \frac{S_c}{\sigma_3} & 0 \geq \sigma_1 \geq \sigma_3 \end{cases} \right) \quad (3.1)$$

Where the maximum and minimum principal stresses are represented by σ_1 and σ_3 ; S_t and S_c are tensile and compressive ultimate strength, respectively. As shown in Figure 3.3, the temperature in the circle with a radius of 10 mm in the middle of panels is increased to 700 °C in 60 s then the middle circle area is kept at 700 °C for 540 s; 700 °C is picked for the maximum temperature since the average safety factor in this condition lies between 1 and 2. This transient thermal analysis is done within 600 s. The input and output energies of the system are equal at 600 s and the whole panel reaches a steady-state condition. Identical temperature distributions for the panels with 3×3 , 5×5 and 7×7 arrays of blocks are observed as each block is perfectly in contact with adjacent blocks (Figure 3.3b to 3.3e). Mesh sensitivity is conducted to assure the reliability of the FEM results. Mesh sizing is set to be 10^{-3} m over the whole panel and on contacts are set to be 8×10^{-4} m. Therefore, the small amount of temperature difference in Figure 3.3a (1-2 °C) is due to the gaps generated to geometries of building blocks where some materials between corners of blocks are removed to achieve interlocking designs. Material removal is causing less than 0.9% difference in the volume of structures due to the gaps.

Table 3.2. Material properties of non-porous alumina ceramics used in FEM [50, 124].

Properties	Value	Properties	Value
Tensile strength	220 (MPa)	Specific heat	880 (J/Kg°C)
Compressive strength	2100 (MPa)	Thermal conductivity	24.6 (W/m.K)
Modulus of Elasticity	303 (GPa)	Thermal expansion coefficient	82.8 ($10^{-7}/^{\circ}C$)
Density	3800 (Kg/m ³)	Static coefficient of friction	0.24

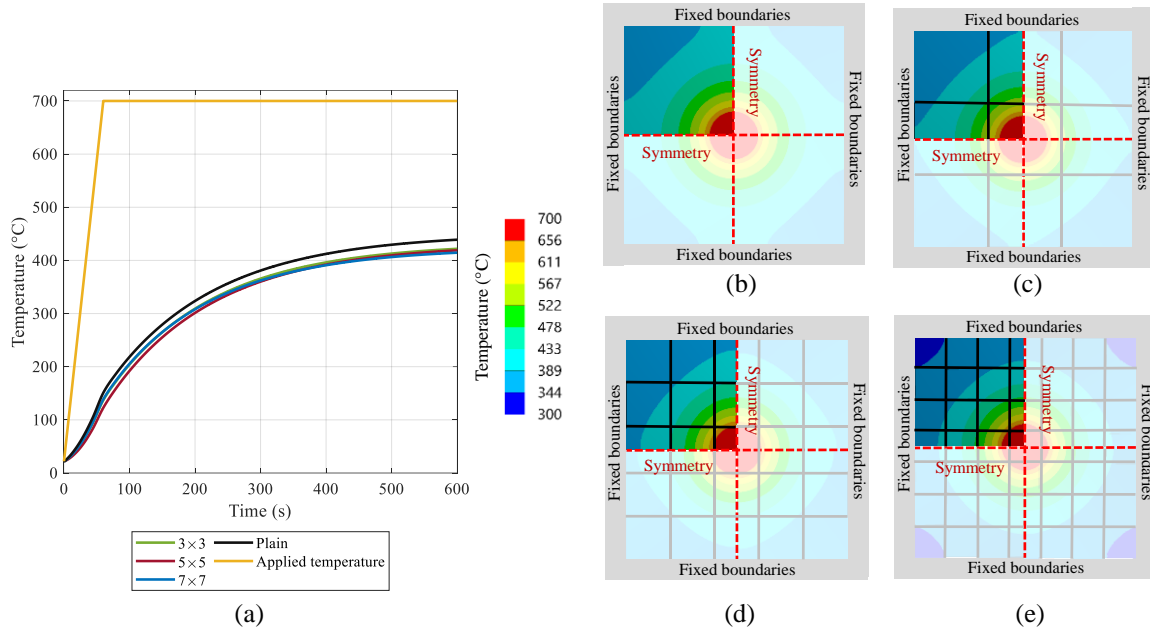


Figure 3.3: Temperature response of ceramic panels: (a) Transient temperature variation; Temperature distribution at the end of the analysis ($t=600$ s) for (b) Plain panel and architected panels with (c) 3×3 , (d) 5×5 and (e) 7×7 arrays of blocks.

Temperature distribution causes distinct thermal expansion at different locations of the panels; for example, the middle tile is exposed to a higher temperature that leads to a higher out-of-plane deflection compared to the others. The out-of-plane deflection is due to in-plane deformation caused by a combination of sliding, thermal buckling and bending. The in-plane thermal stress has been computed by importing the determined temperature distribution to the mechanical module of ANSYS Workbench. The static coefficient of friction between ceramic blocks is set at 0.24 [50]. Different thermal expansion of adjacent tiles causes sliding and energy dissipation through contact. Displacements in all three directions of x , y and z are fixed on all four edges of the ceramic panels and the temporal behavior of the panels is studied. Energy balance is calculated to observe the mechanical performance of the panels [146]:

$$U = Q + W_t \quad (3.2)$$

$$W_t = E_{strain} + E_{FDE} + W_{env} \quad (3.3)$$

where U , Q and W_t are internal energy, thermal energy and mechanical energy, respectively. E_{strain} , E_{FDE} and W_{env} are strain energy, frictional dissipation energy and work on the environment, respectively. Thermal energy stored in the system is determined by the specific heat of alumina ceramic. To compute the internal and thermal energy of the system, ANSYS Fluent is

used. At $t = 600$ s, inlet and outlet of the internal energy of the system are equal and 8.71 kJ energy is stored as internal energy. This 8.71 kJ is separated into thermal energy $Q = 8.58$ kJ (98% of total internal energy) and mechanical energy as $W_t = 0.13$ kJ that consists of three parts: (1) Strain energy that is the mechanical energy stored in the system, (2) Frictional dissipation energy and (3) Work on the surrounding environment by deflection of the architected panel. Mechanical energy is calculated by fixing the whole of the plain panel and setting the displacements in all three directions equal to zero. In this approach, the mechanical energy is equal to the strain energy of the panel as W_{env} and E_{FDE} is set equal to zero. The total amount of energy received by all designed architected panels is the same, leading to equal thermal energy and mechanical energy for all panels. However, strain energy (E_{strain}), frictional dissipation energy (E_{FDE}), and work on the surrounding environment (W_{env}) vary for alternative designed architectures.

3.4 Machine Learning (ML)

ML is an application of artificial intelligence and a data-driven approach to find a pattern in existing data. In this work, ML is used to examine the thermomechanical performance of a series of alternative architected ceramic panels. Interlocking angles and the number of blocks are inputs, while safety factor, max deflection, sliding distances, reaction forces on the boundaries, frictional dissipation and strain energies are outputs of the model. For each of the 3×3 , 5×5 and 7×7 -block architected panels, 100 random designs have been analyzed by FEM. Interlocking angles in the designs are varied from 5° to 25° . The correlation of input parameters to outputs is investigated in the preprocessing step. Normalizing and scaling help the ML models to converge and make the training less sensitive to the scale of features.

Middle architected ceramic blocks interact with four surrounding blocks, while blocks on edges and corners interact with two or three blocks, respectively. The vast design space (Table 3.1) is computationally expensive to be modelled only by using FEM; ML algorithms can assist in exploring all possible designs. Multilayer perceptron (MLP), so-called feedforward artificial neural network for the regression problem (ANN) [60] is employed due to its better performance compared to other models [100] (appendix 1). For this purpose, MLP regressor from Sklearn library is used in Python. Hyperparameters such as the number of hidden layers, the L2 penalty parameter, the initial value for learning rate and the max number of iterations are tuned by conducting a grid search. ReLu activation function has been used due to its higher accuracy than

the logistic activation function. ReLU activation outputs directly the positive input and outputs the negative input to zero [101, 102]. Randomly, 10% of the dataset is picked for the test set and five-fold cross-validation is chosen to prevent overfitting. The mean accuracy of the ML models for predicting each output are reported in 3.A1.

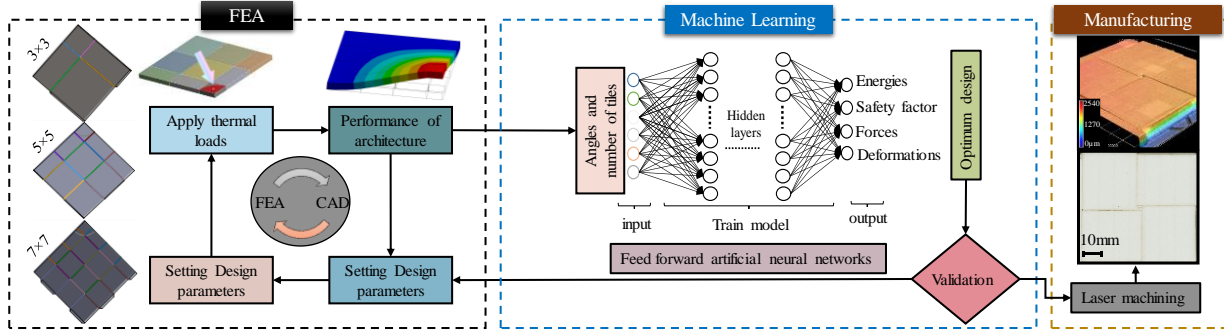


Figure 3.3: Schematic of the algorithm for studying the thermomechanical performance of architected materials. By varying interlocking angles from 5° to 25°, 406875 different architected panels can be produced, which are studied by a Neural Network algorithm (MLP).

3.5 Results and Discussion

In this section, the effects of interlocking angles on the thermomechanical response of architected ceramic panels are studied. All boundary conditions and thermal loads remained unchanged for the sake of comparison of the performance of alternative architected ceramics. First, we compare the responses when all blocks have identical interlocking angles. Then, ML algorithms are used to investigate all possible panels that have building blocks with dissimilar interlocking angles.

Figure 3.5 presents safety factors, reaction forces on boundaries and strain for plain and architected (10° interlocking angle) ceramic panels during a time span of 600 s. While the plain ceramic panel fails after 50 s, all the architected panels remain integrated over the period of the time considered in this study. A higher amount of strain energy inside the plain panel and higher reaction forces on fixed boundaries are observed, resulting in a rapid failure compared to the architected ceramic. Meanwhile, for this architected design, about 3% of the mechanical energy is dissipated through sliding and friction in the constitutive building blocks. The energy dissipation assists the architected panels to resist the same thermal load in a larger time frame. The 7 × 7-block architected panel with uniform distribution of interlocking angle 10° presents a higher safety factor compared to the 3 × 3 and 5 × 5-block architected panels. Architected ceramic panels with alternative interlocking angles are explored in the next section to ensure the

accuracy of the comparison of the thermomechanical performance of panels. It can be concluded that the plain panel performs poorly compared to the designed architectures in terms of failure resistance, the application of higher forces on the boundaries and the development of higher strain energy.

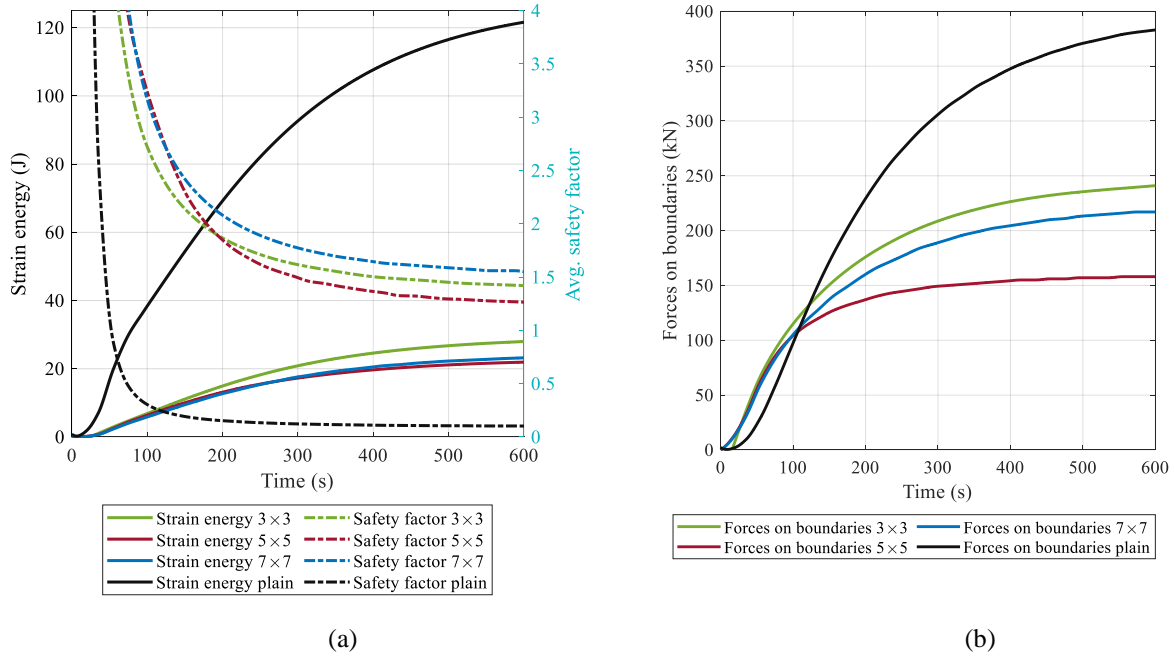


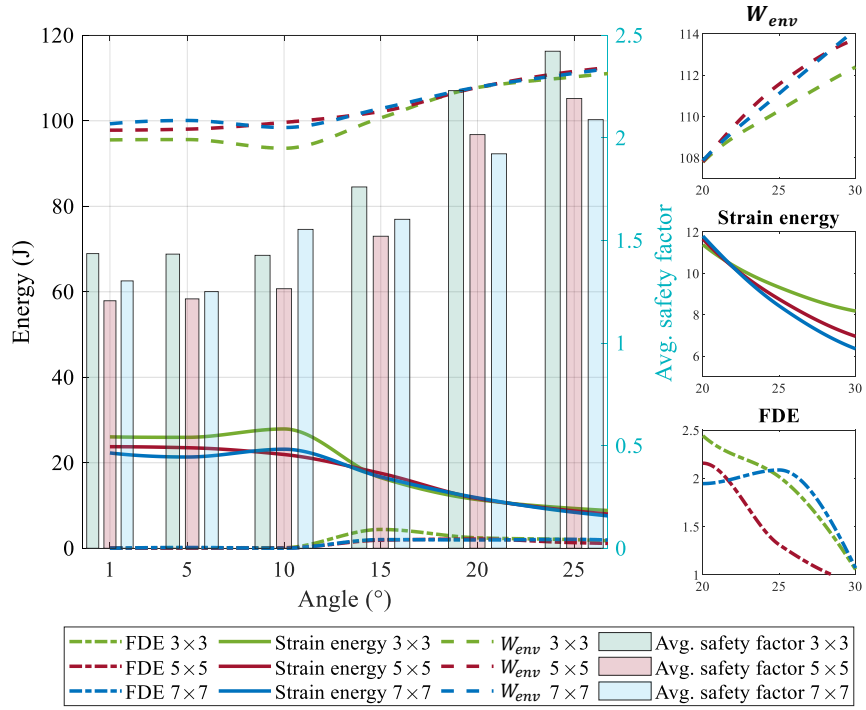
Figure 3.5: (a) Comparing strain energy and safety factor of the architected panels with the plain panel. The plain panel fails earlier than architected designs, and it suffers from a higher amount of stress inside the panel. (b) Comparing reaction forces on fixed boundaries of the architected panels with the plain panel. The plain panel applies higher forces to fixed boundaries.

3.5.1. Architected Designs with Uniform Interlocking Angles

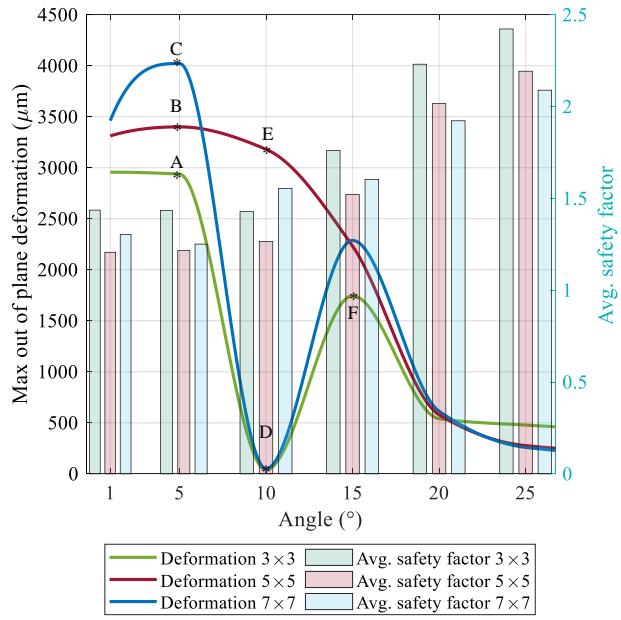
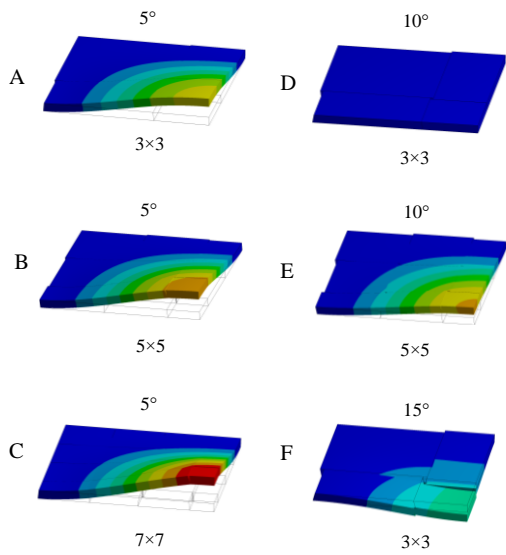
Architected panels with a uniform distribution of interlocking angles are studied here. The analysis considers all blocks having the uniform interlocking angles; however, they can be varied from 5° to 25° . In Figure 3.6, strain energy, frictional dissipation energy (FDE), reaction force and out-of-plane deformation are presented. As seen in Figure 3.6a, the values of FDE are negligible for interlocking angles of less than 10° . At 10° interlocking angle, FDE starts to increase and a drop is observed in the strain energy, indicating that the sliding begins at 10° . Frictional sliding mechanism is one of the key factors to have better resistance to failure. Stresses and energies inside the panels are reduced when more energy is dissipated through friction. For interlocking angles

larger than 15° FDE in the 3×3 -block panel is higher and consequently, its average safety factor is higher than the 5×5 and 7×7 -block panels.

In general, less strain energy in the panels results in a lower reaction force on the boundaries. As shown in Figure 3.6c, for the interlocking angles between 15° and 30° , the 3×3 -block panel has a lower force on the boundaries and a higher safety factor compared to the other panels. Out-of-plane deformation of the panels (Figure 3.6b) with interlocking angles more than 15° is less than their counterparts with lower interlocking angles. At 10° , a drop in the out-of-plane deformation is observed because the panel experiences a locking behavior that hinders blocks from being deformed. This trend is different for the 5×5 -block architected panels because the deflection depends on the area where the temperature is applied (a circle with a diameter of 10 mm that is $\sim 3\%$ of the total area of the top surface). Except the 3×3 -block panel, the heat is applied to more than 1 block. As expected for the higher interlocking angles, more sliding occurs as shown in Figure 3.6d. The results show that the sliding distance, which represents the sum of the path of the movement, is highly correlated to the panel safety factor. Even though the 3×3 -block architected panel has less contact areas, this panel reveals more sliding and a higher safety factor. Higher sliding is a representation of dissipating more energy, the energy that can be stored in the panel causing stress inside the panel. In the next section, ML algorithms are adopted to explore the dependence of the architectures with variable angles on the outputs.



(a)



(b)

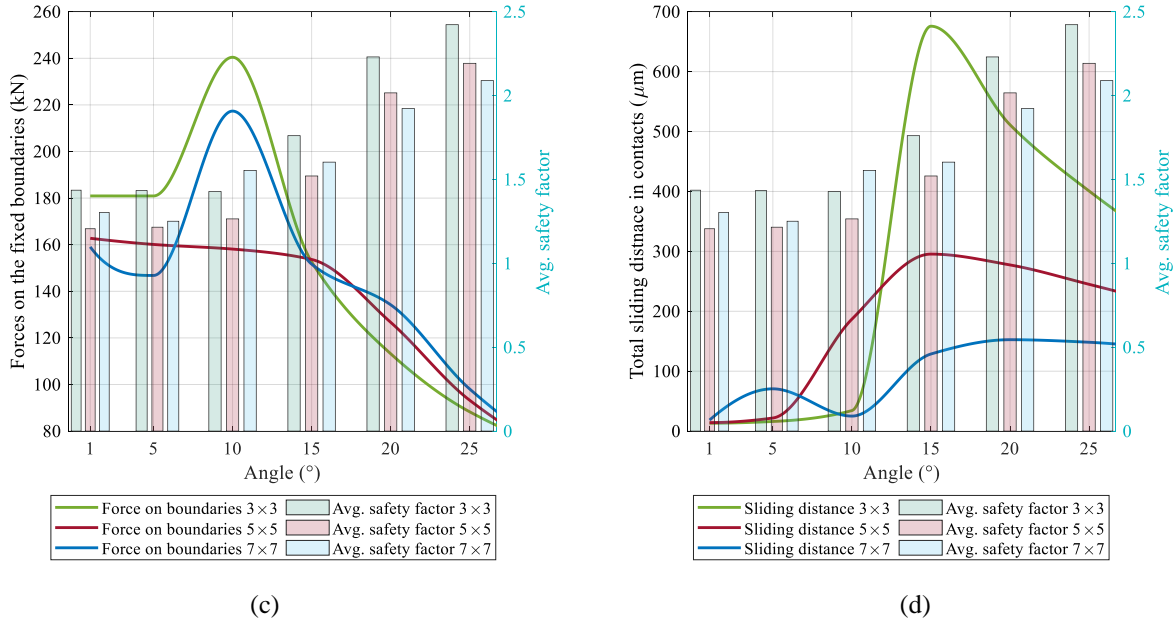


Figure 3.6: Comparing the performance of architected designs with the uniform distribution of the interlocking angles. (a) Energy comparison and safety factor, (b) Out-of-plane deformation, (c) Force reaction on fixed boundaries and (d) Total sliding distance of adjacent blocks over the whole of the architected panel.

3.5.2. Exploring Designs with Variable Angles using Machine Learning

Data from FEM is imported to ML models to find better-performing architected panels with respect to each output (e.g. strain energy and out-of-plane deformation). These panels are made concerning the accuracies presented in 3.3. To enhance the quality of data, preprocessing has been done over ML models. The preprocessing includes determining the correlation of each interlocking angle to the outputs. Low correlation can reduce the accuracy of the ML models. Exploring correlation indicates that some of the interlocking angles do not affect outputs; for example, the interlocking angle 2 (A_2) has a negligible correlation to the frictional dissipation energy of the 3×3 -block architected panel. These slightly correlated angles are removed in the training process as identified as θ in Table 3.3. Different numbers of building blocks as inputs need three different ML models (see Section 4) with specific hyperparameters to be developed. In Figure 3.7, correlations between inputs and outputs are shown in different designs. It is observed that interlocking angles in structures with a higher number of building blocks have less correlation to the outputs (Figures 3.7e and 3.7f). This can be addressed by having a small amount of training data for the 7×7 -block panel compared to the 3×3 -block panel.

Highly correlated parameters can reveal great information about which interlocking angles should be controlled in each architected panel. For example, all four interlocking angles in the 3×3 -block panel have a higher negative correlation to the total strain energy over the whole panel, suggesting small interlocking angles bring a higher amount of strain energy. Maximum and minimum strain energies, safety factor, total frictional dissipation through contacts, sliding distances, out-of-plane deformation and reaction force on boundaries are presented. ML algorithms suggest a series of designs that can achieve maximum or minimum of the aforementioned outputs. In this regard, panels with more similar interlocking angles are selected since they are more favorable in terms of manufacturing [147] (see Figure 3.A2). Some interlocking angles have a small impact on the output because of that any values can be picked for those angles with θ in Table 3.3.

Table 3.3. Machine learning algorithms for architected ceramic designs with minimum and maximum outputs. Each output and the mean accuracy for each model are reported.

3×3-block panel	A₁	A₂	A₃	A₄	A₅	A₆	A₇	A₈	Mean accuracy (%)	R² error
Max strain energy	5°	5°	5°	5°	--	--	--	--	84	0.96
Min strain energy	25°	25°	25°	25°	--	--	--	--		
Max deformation	5°	5°	25°	15°	--	--	--	--	73	0.77
Min deformation	25°	25°	5°	25°	--	--	--	--		
Max avg. safety factor	25°	25°	25°	25°	--	--	--	--	94	0.95
Min avg. safety factor	5°	5°	5°	25°	--	--	--	--		
Max total FDE	15°	θ	20°	15°	--	--	--	--	65	0.32
Min total FDE	5°	θ	5°	5°	--	--	--	--		
Max total sliding distance	15°	20°	θ	10°	--	--	--	--	72	0.93
Min total sliding distance	5°	5°	θ	5°	--	--	--	--		
Max force on the boundaries	5°	5°	15°	5°	--	--	--	--	74	0.94
Min force on the boundaries	25°	25°	25°	25°	--	--	--	--		
5×5-block panel	A₁	A₂	A₃	A₄	A₅	A₆	A₇	A₈	Mean accuracy (%)	R² error
Max strain energy	5°	5°	5°	5°	5°	5°	--	--	85	0.71
Min strain energy	25°	25°	25°	25°	25°	25°	--	--		
Max deformation	5°	25°	5°	25°	5°	5°	--	--	86	0.70
Min deformation	25°	5°	25°	5°	25°	25°	--	--		
Max avg. safety factor	25°	5°	25°	5°	25°	25°	--	--	85	0.88
Min avg. safety factor	5°	5°	5°	5°	5°	5°	--	--		
Max total FDE	25°	5°	5°	5°	5°	5°	--	--	60	0.85
Min total FDE	5°	25°	25°	25°	5°	25°	--	--		

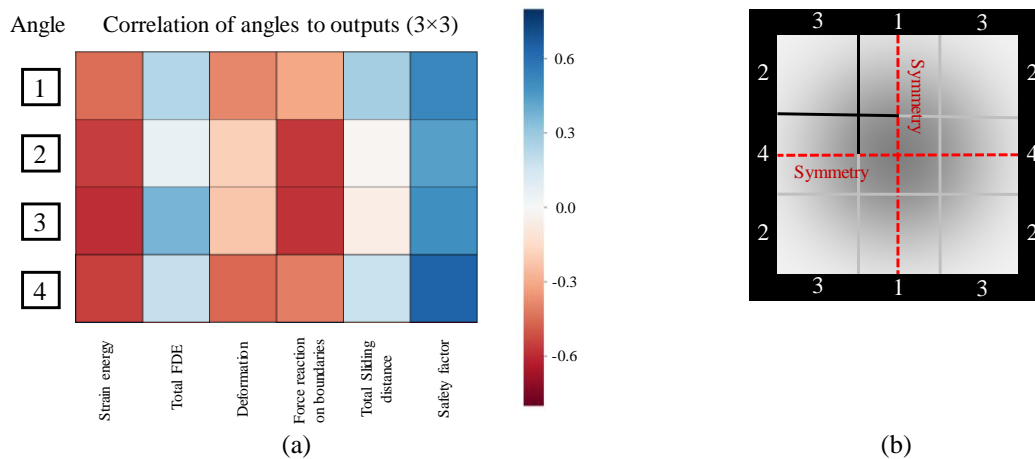
Max total sliding distance	5°	25°	5°	θ	25°	25°	--	--	71	0.32
Min total sliding distance	5°	5°	5°	θ	5°	5°	--	--		
Max force on the boundaries	5°	5°	5°	5°	5°	5°	--	--	70	0.89
Min force on the boundaries	25°	25°	25°	25°	25°	25°	--	--		
7×7-block panel	A₁	A₂	A₃	A₄	A₅	A₆	A₇	A₈	Mean accuracy (%)	R² error
Max strain energy	5°	5°	25°	5°	25°	5°	5°	25°	60	0.62
Min strain energy	25°	15°	15°	25°	20°	25°	25°	15°		
Max deformation	5°	25°	25°	5°	θ	5°	5°	θ	67	0.36
Min deformation	5°	5°	5°	5°	θ	25°	25°	θ		
Max avg. safety factor	25°	25°	25°	25°	5°	25°	25°	5°	80	0.71
Min avg. safety factor	5°	5°	5°	5°	5°	5°	5°	5°		
Max total FDE	5°	25°	5°	25°	θ	25°	25°	θ	54	0.13
Min total FDE	25°	5°	20°	5°	θ	5°	5°	θ		
Max total sliding distance	25°	θ	5°	θ	5°	25°	θ	25°	57	0.13
Min total sliding distance	25°	θ	25°	θ	25°	10°	θ	5°		
Max force on the boundaries	5°	5°	25°	25°	5°	θ	25°	25°	75	0.58
Min force on the boundaries	20°	15°	5°	5°	25°	θ	20°	5°		

Grey highlight in this table represents the structures that have been further investigated with FEM.

θ represents the angles that have a small correlation to the outputs.

A₁-A₈ represent the angles which are shown in Figure 3.7.

Panels with a greater number of inputs need more data to predict accurately. The mean accuracy for the output parameters in the 7 × 7-block architected panel is much less than 3 × 3 and 5 × 5-block panels; this indicates that training a model for the 7 × 7-block panel is more challenging than the other architected panels.



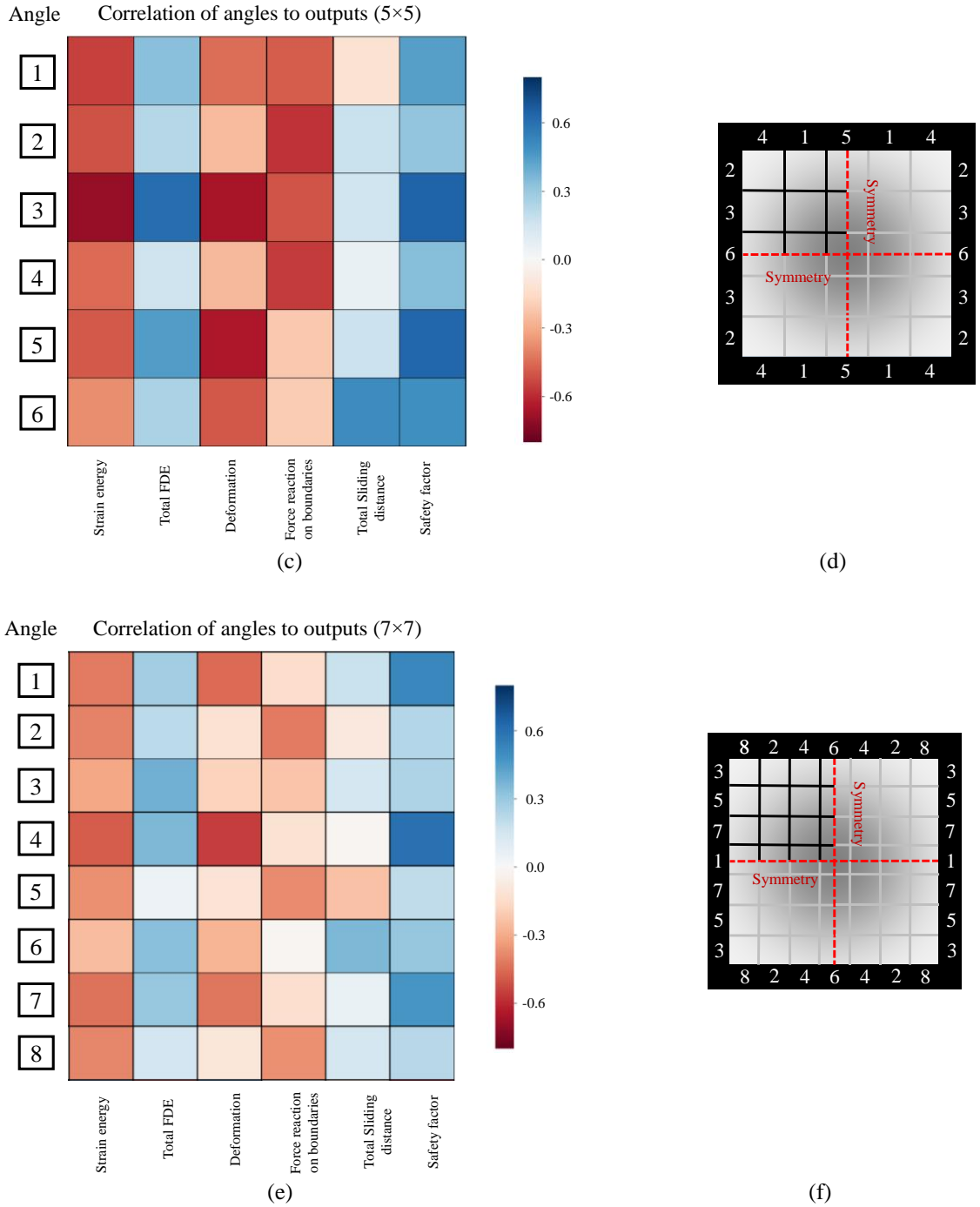
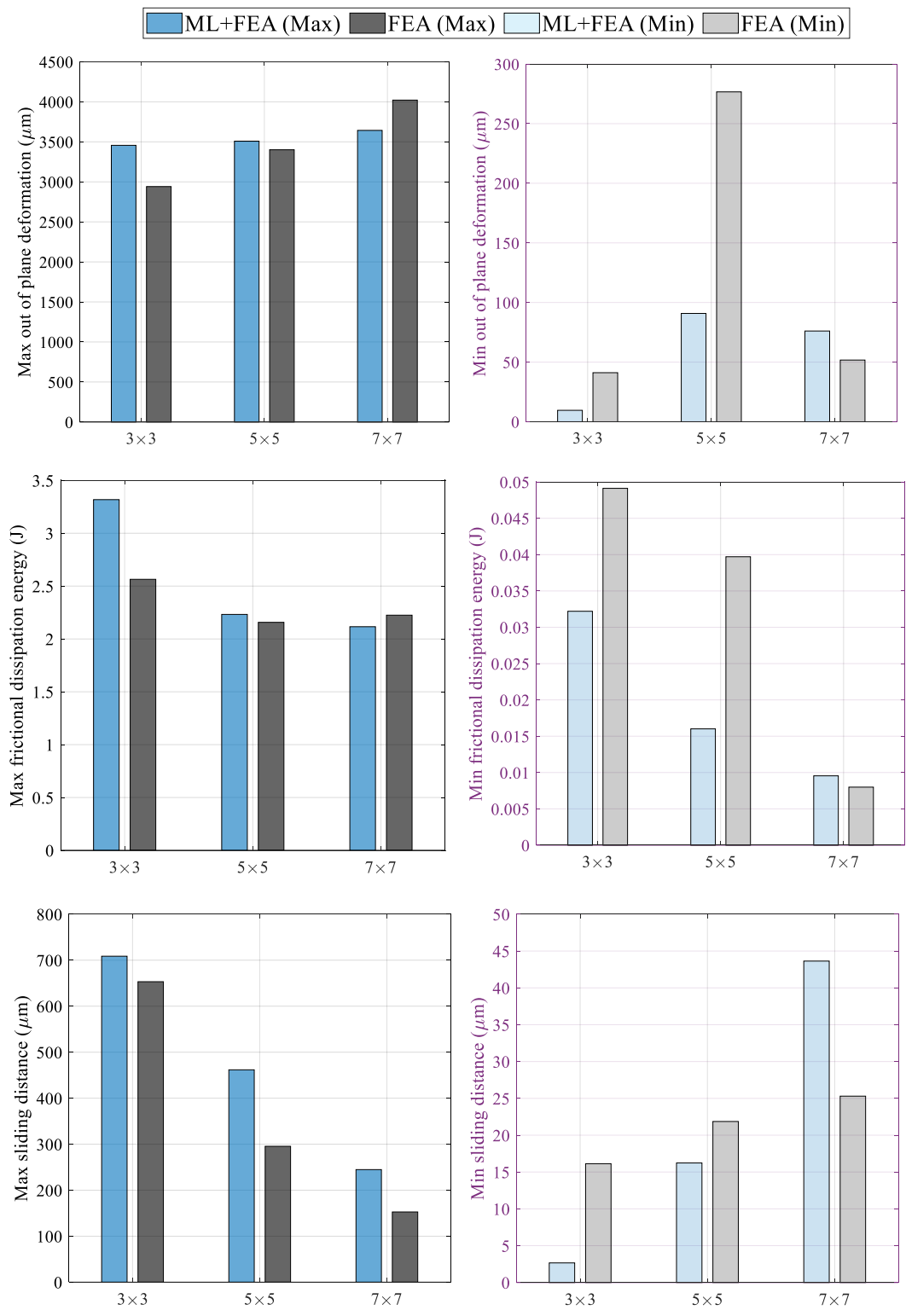


Figure 3.7: (a, c, e) Correlation between input parameters as interlocking angles and output parameters. Schematic of (b) the 3×3-block architected, (d) 5×5-block architected panel, (f) 7×7-block architected panel and symmetry planes. Each number represents a different interlocking angle.

Here, we explore the accuracy of predicted output values by ML through comparison with the FEM results. In Figure 3.8, the performance of the suggested varied-angle architected panels from ML is compared with the FEM results for the architected panels with uniform interlocking

angles across the panel. The maximum and minimum values of the outputs are reported in Figure 3.8. In most cases, ML could increase the maximum and decrease the minimum of outputs. However, ML could not increase the maximum out-of-plane deformation and frictional dissipation energy (FDE) in the 7×7 -block architected panel due to the low amount of training data. The deformations and FDE in the 3×3 and 5×5 -block panels can be increased by using ML and designing varied-angle architected panels. In the 3×3 -block panel, 15%, 7% and 30% improvements in maximum out-of-plane deformation, sliding distance and frictional dissipation energy are observed, respectively. In addition, 70%, 80% and 30% reductions in the minimum out-of-plane deformation, sliding distance, and frictional dissipation energy are observed, respectively. In the 5×5 -block panel, 3%, 35% and 4% improvements in maximum out-of-plane deformation, sliding distance and FDE are observed, respectively. 70%, 15% and 52% reductions in minimum out-of-plane deformation, sliding distance and frictional dissipation energy are noticed, respectively. Machine learning is not providing new designs to maximize or minimize the force on the boundaries, strain energy, and safety factor. Proposed designs from the ML algorithms are explored by FEM to further verify the ML predictions. For this purpose, three outputs from Table 3.3 (highlighted in grey), which are FDE and sliding distance in the 3×3 -block panel and out-of-plane deformation in the 5×5 -block panel, are chosen to be further investigated. These outputs are chosen due to their high accuracy.



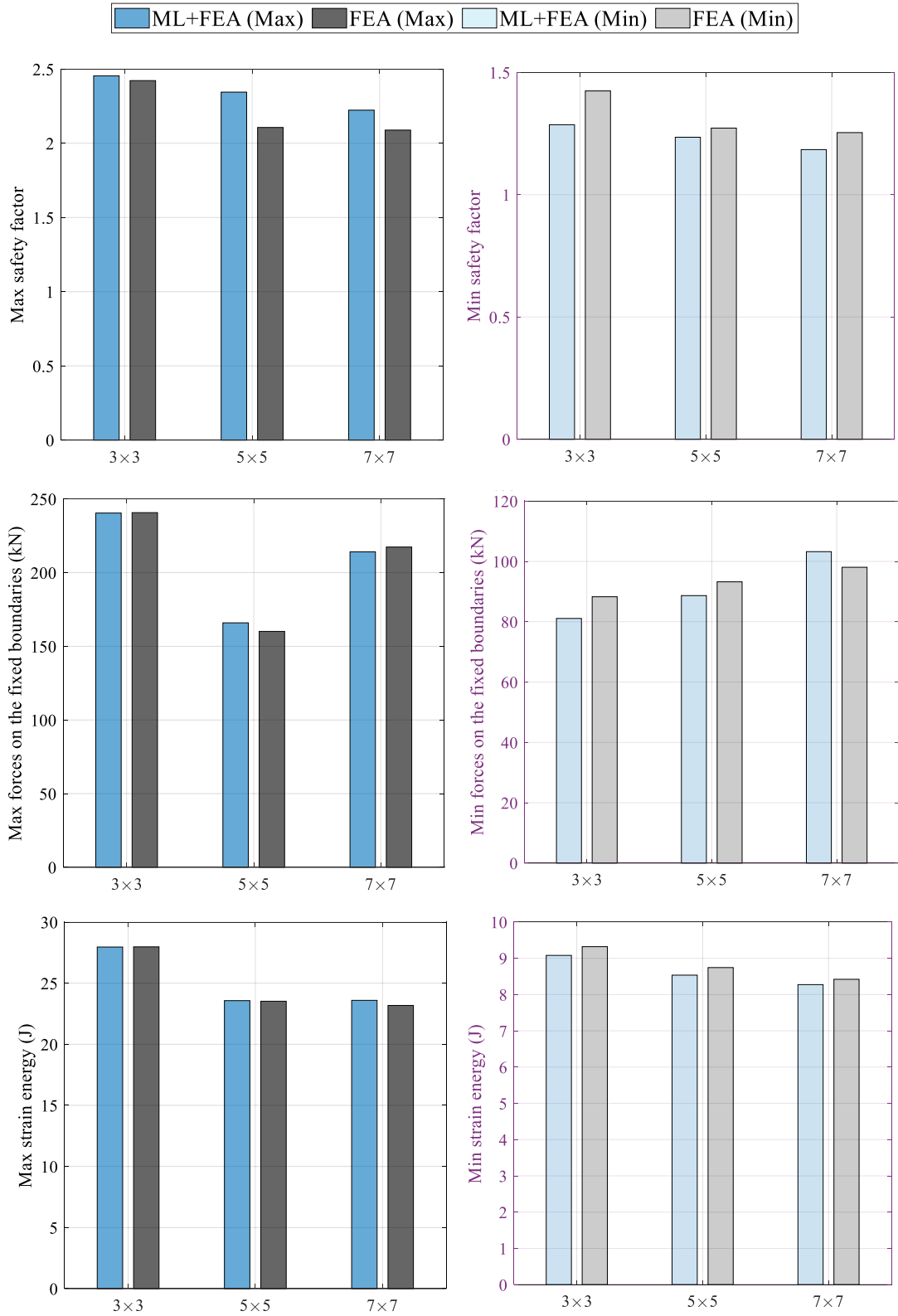
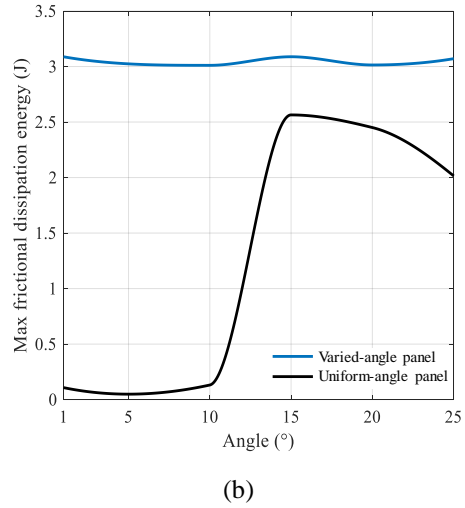
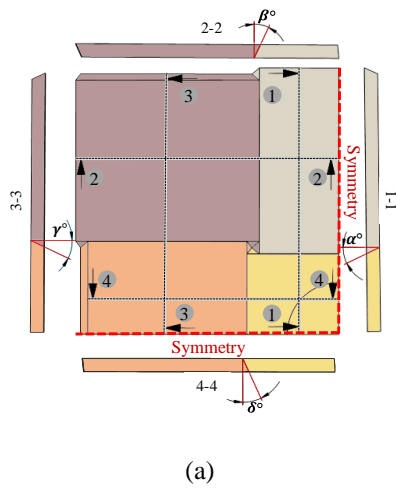


Figure 3.8: Comparison of results obtained by machine learning to results without using machine learning.

To achieve the maximum frictional dissipation energy for varied-angle architecture panels of 3×3 , ML suggested selecting angle 1 (α) = 15° , angle 3 (γ) = 20° and angle 4 (δ) = 15° . Interlocking angle 2 (β) in this design can be varied due to a small correlation to the frictional dissipation energy (FDE). Figure 3.9b indicates the effect of changing interlocking angle 2 (β) on the frictional dissipation energy (FDE) of the panel. This horizontal blue line indicates that interlocking angle 2 (β) does not play a great role in the maximization of FDE. Also, it can be concluded that the varied-angle architected panels found from ML increase the maximum of outputs and decrease the minimum of outputs (the horizontal blue line is higher than the black line). The same logic can be used for the sliding distance and the varied-angle panel with $\alpha = 15^\circ$, $\beta = 20^\circ$, γ and $\delta = 10^\circ$ (see Figure 3.9c). In Figure 3.9d, the out-of-plane deformation of the varied-angle panel with the 5×5 arrays of blocks is compared with the uniform-angle panel. It is shown that the maximum out-of-plane deformation of the 5×5 -block architected panel is 3% increased.



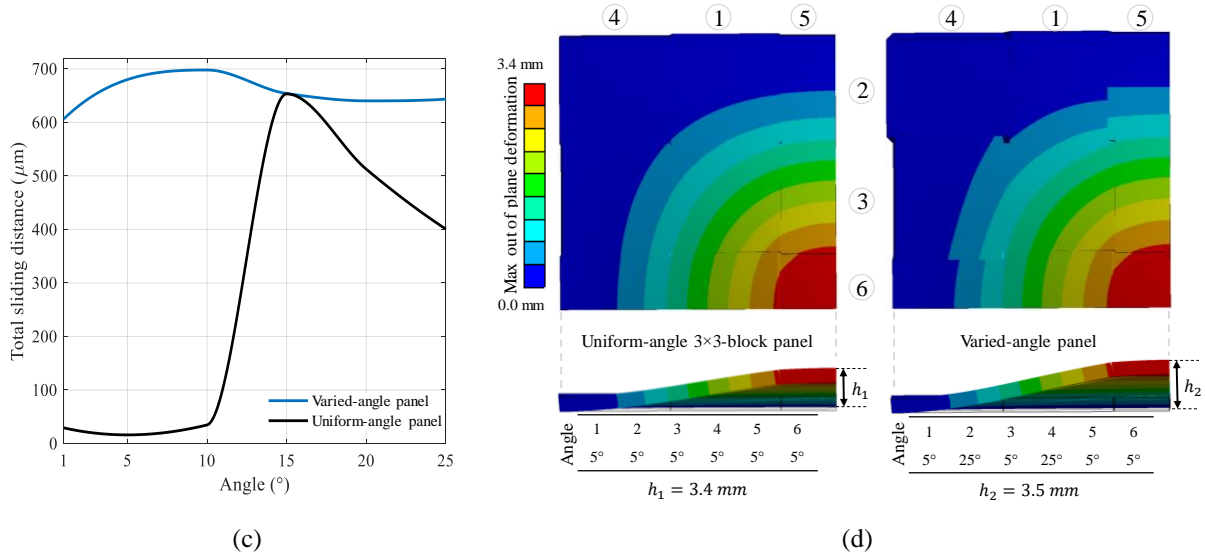


Figure 3.9: Comparison of the varied-angle and uniform-angle architectural panels. (a) Schematic of 3×3 -block panel with varied-angle; $\alpha = \text{angle 1}$, $\beta = \text{angle 2}$, $\gamma = \text{angle 3}$, $\delta = \text{angle 4}$. (b) Suggested varied-angle panel to maximize frictional dissipation energy; $\alpha = 15^\circ$, $\beta, \gamma = 20^\circ$, $\delta = 15^\circ$. The results of the varied-angle design are shown in the blue line, which shows a change in β does not play a great role in the total sliding distance. (c) The suggested varied-angle panel, $\alpha = 15^\circ$, $\beta = 20^\circ$, $\gamma, \delta = 10^\circ$, to maximize the sliding distance. The results of the varied-angle design are shown in the blue line, which shows a change in γ does not play a great role in the total sliding distance. (d) Comparison of maximum out-of-plane deformation in the 5×5 -block architectural panels with the varied-angle and uniform-angle designs.

3.6 Concluding Remarks

Despite the excellent thermal stability of ceramics, most of the research endeavors have focused on evaluating the mechanical performance of architected ceramics under quasi-static or impact loading rather than a thermal stimulus. In this study, finite element modeling is used to evaluate the thermomechanical performance of architected ceramics made of interlocked building blocks. It is shown that the architected designs outperform monolithic ceramics in the energy dissipation and results in an 80% strain energy reduction that causes less stress in the structure and postpones the structural failure, a 67% reduction in forces on the fixed boundaries, and a 90% increase in the safety factor. We have proposed a systematic approach by adopting a hybrid ML-FEM algorithm to design high-performance architected ceramics experiencing thermal loads. The thermomechanical performance of the architected ceramics is first explored using FEM, and then the ML models are trained using the FEM data of hundreds of randomly generated interlocked architectures. While the proposed approach may need a high amount of the training datasets to reach higher accuracy, this algorithm presented promising results that are verified by FEM. In this analysis, the out-of-plane deformation, strain and frictional dissipation

energies, reaction forces, safety factor and sliding distances of adjacent blocks in the architected ceramics made of interlocked building blocks are explored. MLP algorithm is used to find the designs with maximum and minimum outputs by changing the angle of cuts between building blocks. It is shown that the suggested designs from ML algorithms perform better for the desired output. For example, these designs can dissipate 30% more energies through friction and 7% more sliding between blocks compared to the interlocked architectures with constant cutting angles and will result in superior thermomechanical performance. In addition, the interlocked angles and architectures generated in the current method can serve as an initial guess for further investigations in practically important cases such as impact or thermal shock applications. This algorithm can be readily adopted in broad applications.

It is demonstrated that the architected ceramic panels perform better in a thermomechanical environment compared to the monolithic ones. ML tool is easy to use and computationally efficient to run a parametrical study and investigate the effects of architectural parameters on performance. This new approach is orders of magnitude computationally faster than conventional methods, making the search for high-performance materials in a vast design space possible. In this algorithm higher number of inputs act as limitations; for example, it is harder to train a model for the 7×7 -block panel. In addition, instead of only using FEM data for the ML algorithms, there is a possibility to use data from experiments and combine it with FEM data to increase the accuracies of ML models. In future studies, experimental data can be produced by employing laser cutting techniques to validate our results (see appendix, Figure 3.A2 [103, 147]). The novel paradigm offered by advanced additive/subtractive manufacturing along with machine learning tools can facilitate the development of advanced ceramic materials that can prevail material property tradeoffs found in monolithic materials (e.g. toughness in brittle materials). This work not only provides a new method that harnesses simulation data and machine learning to potentially design future bioinspired, architected and composite materials in an experience-free and systematic manner but also opens a new avenue to address various inverse design problems in different industrial sectors such as aerospace, automotive, transportation and energy.

3.7 Acknowledgments

Authors acknowledge the financial support by National Research Council Canada through Security materials Technology and New Beginnings Initiative – Ideation Fund to H. Yazdani Sarvestani, B. Ashrafi, and A.H. Akbarzadeh. H. Yazdani Sarvestani was supported by a FRQNT (Fonds Nature et technologies) postdoctoral award. A.H. Akbarzadeh acknowledges the financial support by Natural Sciences and Engineering Research Council of Canada through NSERC Discovery Grant (RGPIN-2016-0471) and the Canada Research Chairs program.

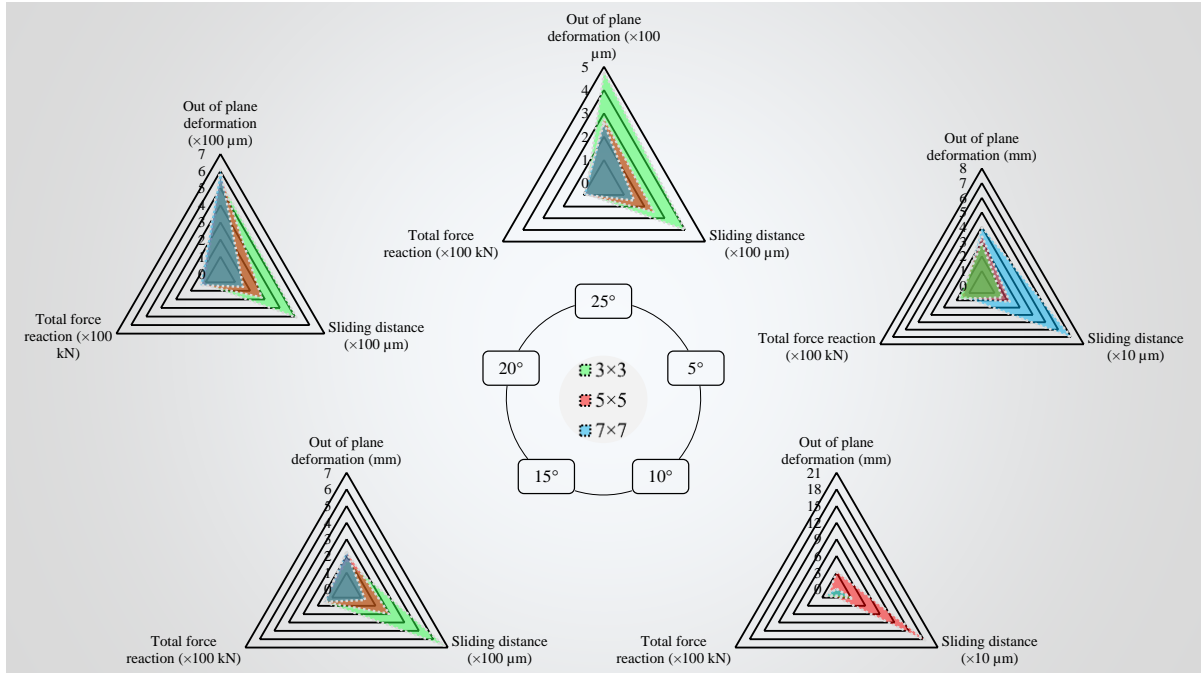
3.8 Appendix

The performance of ML models concerning accuracies is compared in Table 3.A1. For this purpose, MATLAB Regression Learner toolbox is used. It is shown that MLP has lower Root Mean Square Error (RMSE) and better performance compared to Linear Regression, Tree, SVM and Gradient Boosting models.

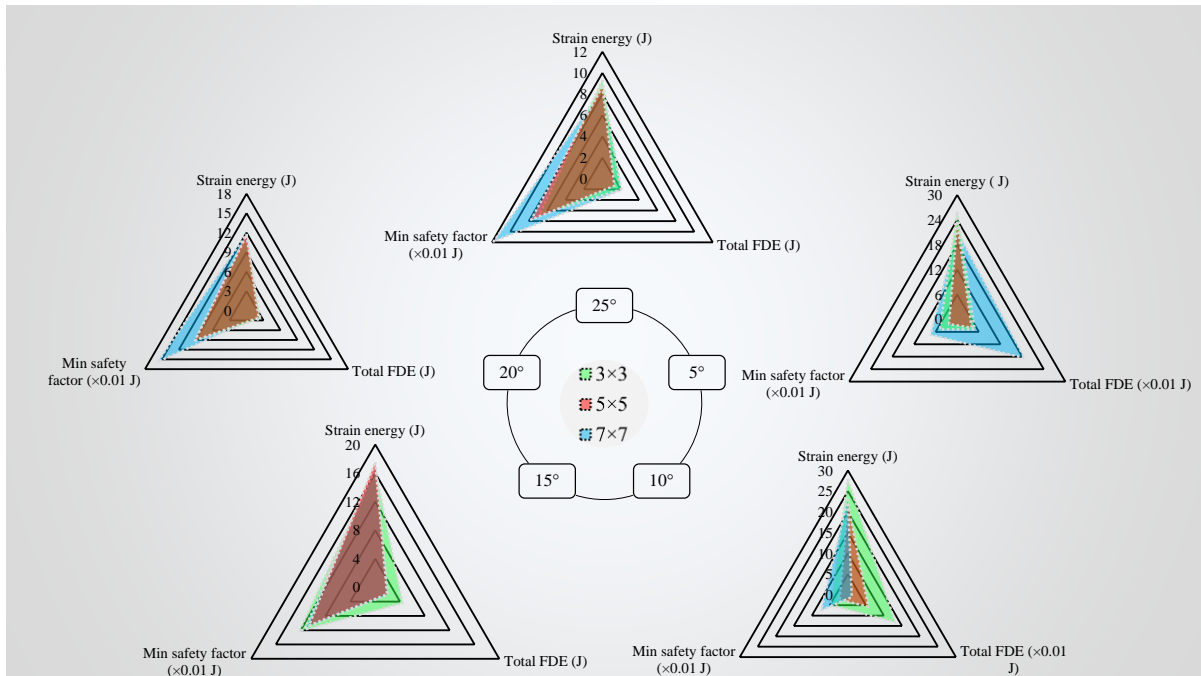
Table 3.A1. RMSE comparison of ML models.

RMSE	Linear regression	Tree	SVM	Gradient Boosting	MLP
3×3	1.54	2.41	1.33	1.56	0.47
5×5	1.83	1.90	1.36	1.18	0.57
7×7	1.25	1.80	0.88	1.12	0.62

In Figure 3.A1, the results presented in Section 5.2 are shown in triangular radar graphs. These graphs can facilitate a comparison of the performance of alternative architected panels for specific applications.



(a)



(b)

Figure 3.A1: Comparing uniform-angle architected designs and their output parameters for the panel selection process in a defined application. (a) Out-of-plane deformation, force reaction on fixed boundaries and sliding distances are compared. (b) Strain energy, total frictional dissipation energy and minimum safety factor are compared.

The laser cutting method, named wobbling, using a picosecond fiber laser, has recently been adopted for defect-free manufacturing of industrial-grade alumina ceramics [8]. The developed

laser system is suitable for the fabrication of engineered net shaping material systems. An example of topologically interlocked ceramics has been manufactured and is shown in Figure 3.A2.

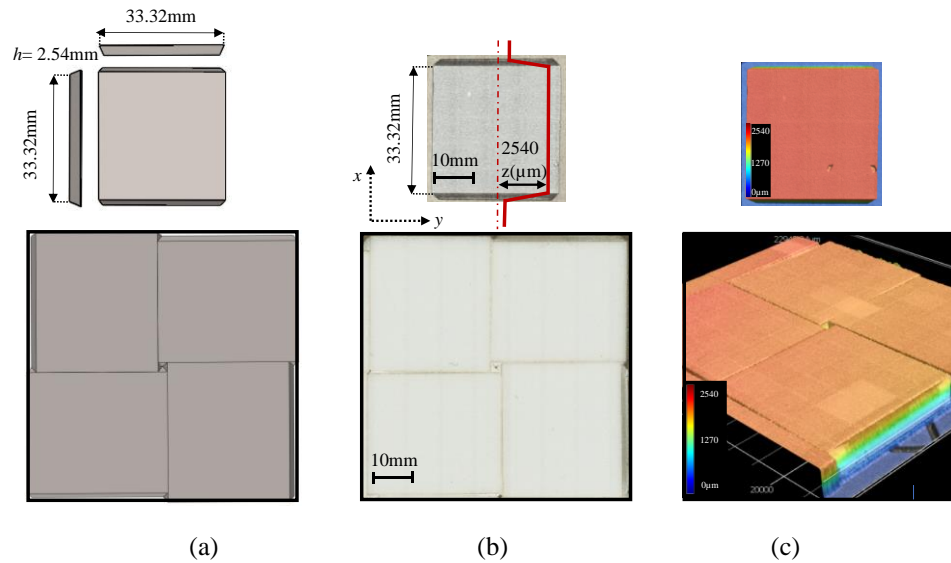


Figure 3.A2: Manufacturing of interlocked ceramic samples using laser cutting. (a) CAD modeling of the truncated tetrahedral ceramic block in TIMs. (b) Truncated tetrahedral ceramic block. (c) 3D laser scanning microscopy image and topography.

4 Summary, Discussion and Recommendation for Future Studies

4.1 Summary and Discussion

A thorough review of existing literature over bioinspired architected materials and machine learning algorithms and their usage in manufacturing and designing architected materials provided in Chapter 2 for the readers to prepare them for the manuscript provided in Chapter 3. According to the literature review, a gap in the analysis of architected materials (especially topologically interlocked structures) under thermal loads was observed and the new idea of using Machine learning for the design process was developed. Next, in Chapter 3, Finite Element Modeling was conducted over the thermomechanical performance of Topologically Interlocked architected ceramic samples. In the first section of the analysis, we focused on evaluating the energies, including strain energy, work, frictional dissipation energy, out-of-plane deformation, sliding distance, forces on the boundaries and safety factor in plain samples and samples with 3×3 , 5×5 and 7×7 number of tiles in topologically interlocked designs. The analysis indicates that only ~3% energy is dissipated through frictions between contacts of tiles; however, this small amount of energy assisted the architected designs to achieve 80% reduction in the strain energy, a 67% reduction in forces on the fixed boundaries, and a 90% increase in the safety factor, leading to the structural failure delay compared to plain ceramic samples. To further increase the thermomechanical performance of architected ceramic samples, varied-angle interlocked panels and uniform-interlocked panels with 3×3 , 5×5 and 7×7 number of tiles studied.

Considering all possible combinations of designs for varied-angle panels resulted in 400k designs that are not feasible and efficient to be modeled only using finite element modelings. Machine learning algorithms were employed on the limited number of data from FEM analysis and predicted the thermomechanical performance of the vast design space. Out of all predictions, the designs with maximum and minimum strain energy, frictional dissipation energy, out-of-plane deformation, sliding distance, forces on the boundaries and safety factor were reported. In the 3×3 -block panel, 15%, 7% and 30% improvements in maximum out-of-plane deformation, sliding distance and frictional dissipation energy are observed, respectively. In addition, 70%, 80% and 30% reductions in the minimum out-of-plane deformation, sliding distance, and frictional dissipation energy are observed, respectively. In the 5×5 -block panel, 3%, 35% and 4% improvements in maximum out-of-plane deformation, sliding distance and FDE are observed, respectively. 70%, 15% and 52% reductions in minimum out-of-plane deformation, sliding distance and frictional dissipation

energy are noticed, respectively. Out of all the designs with improvements, three different cases were selected to be validated by doing another round of finite element analysis. Finally, the validated designs could dissipate 30% more energies through friction and 7% more sliding between blocks than the interlocked architectures with uniform cutting angles. A straightforward benefit ML brought to this study was promoting the efficiency of materials designs with FEM data. Exploring a massive design space of novel architected materials was too complicated to achieve using only FEM analysis. Instead, the hybrid ML-FEM design approach could incorporate materials and mechanical features during the preprocessing of input data, learn the relationship between materials structures and mechanical behaviors during training and could provide targeted designs using the trained models.

4.2 Recommendation for future studies

In this study, we studied the material designs using machine learning and finite element modeling. Studies in computer science, material science and mechanical engineering have been flourished over the past decades. Now it is time to combine the ideas. The possible recommendations for future studies are summarized as follow:

1. The hybrid ML-FEM design algorithm showed a promising approach for investigating and developing new designs; however, experimental tests are needed to strengthen and validate the simulations' results. According to the pandemic limitations in 2020 and 2021, the designs provided in this research could not be tested; however, the interlocked samples could be manufactured using picosecond laser machines. The input parameters provided on Chapter 2 can produce the desired angle of cuts. For validation of the results deflection and force on boundaries can be evaluated by the fixture provided in Chapter 2. Thermomechanical testing can be done at NRC experimental center in Ottawa and the results can be used for validation of the models.
2. The laser cutting of architected ceramics is a challenging procedure and only a small number of research centers have access to the picosecond laser cutting machines. The algorithm developed in this study is not limited to architected ceramic panels. 3D printing machines available in the labs are valuable facilities for manufacturing interlocking samples and other architecture materials. In this way, the designs provided by ML-FEM algorithms can easily be validated by simple mechanical testing on 3D printed samples.

3. In this work, we focused on the mechanical performance of architected materials in high-temperature environments. The algorithm can be employed in different applications, and a specific design will be developed for a specific application. For example, for developing architected materials for impact application, the same procedure can be employed.
4. Theory-guided data science (TGDS) is an emerging paradigm that aims to leverage the wealth of scientific knowledge for improving the effectiveness of data science models. The combination of mathematical models of scientific knowledge with finite element analysis and experimental data will further improve the effectiveness and accuracy of machine learning algorithms.
5. A convolutional neural network (CNN or ConvNet) is a class of deep neural networks most commonly applied for analyzing visual imagery. In this research, we imported the data as numeric input; however, the shape of designs can be imported to the ML models as visual images to find a design with better characteristics.

References

1. Ritchie, R.O., *The conflicts between strength and toughness*. Nat Mater, 2011. **10**(11): p. 817-22.
2. Chang, M.-K., *Mechanical properties and thermal stability of low-density polyethylene grafted maleic anhydride/montmorillonite nanocomposites*. Journal of Industrial and Engineering Chemistry, 2015. **27**: p. 96-101.
3. Meyers, M.A., et al., *Biological materials: structure and mechanical properties*. Progress in Materials Science, 2008. **53**(1): p. 1-206.
4. Yao, N., et al., *Organic–inorganic interfaces and spiral growth in nacre*. 2009. **6**(33): p. 367-376.
5. Naleway, S.E., et al., *Structure and mechanical properties of selected protective systems in marine organisms*. Mater Sci Eng C Mater Biol Appl, 2016. **59**: p. 1143-1167.
6. Barthelat, F., et al., *On the mechanics of mother-of-pearl: A key feature in the material hierarchical structure*. Journal of the Mechanics and Physics of Solids, 2007. **55**(2): p. 306-337.
7. Abid, N., J.W. Pro, and F. Barthelat, *Fracture mechanics of nacre-like materials using discrete-element models: Effects of microstructure, interfaces and randomness*. Journal of the Mechanics and Physics of Solids, 2019. **124**: p. 350-365.
8. Maas, M.C., et al., *Built to last: the structure, function, and evolution of primate dental enamel*. 1999. **8**(4): p. 133-152.
9. Shafaroudi, A.A. and S. Rankohi, *STR-854: MULTIFUNCTIONAL AND MULTIPHYSICS MATERIALS AS LOAD-BEARING STRUCTURAL COMPONENTS*. 2016.
10. Sundar, V.C., et al., *Fibre-optical features of a glass sponge*. 2003. **424**(6951): p. 899-900.
11. Wegst, U.G., et al., *Bioinspired structural materials*. Nat Mater, 2015. **14**(1): p. 23-36.
12. Chen, P.-Y., J. McKittrick, and M.A.J.P.i.M.S. Meyers, *Biological materials: functional adaptations and bioinspired designs*. 2012. **57**(8): p. 1492-1704.
13. Gu, G.X., et al., *Bioinspired hierarchical composite design using machine learning: simulation, additive manufacturing, and experiment*. 2018. **5**(5): p. 939-945.
14. De Luna, P., et al., *Use machine learning to find energy materials*. 2017, Nature Publishing Group.
15. Gu, G.H., et al., *Machine learning for renewable energy materials*. 2019. **7**(29): p. 17096-17117.
16. Liu, H., et al., *Machine learning for glass science and engineering: A review*. 2019: p. 119419.
17. Chen, C.-T. and G.X.J.M.C. Gu, *Machine learning for composite materials*. 2019. **9**(2): p. 556-566.
18. Chen, G., et al., *Machine-learning-assisted de novo design of organic molecules and polymers: opportunities and challenges*. 2020. **12**(1): p. 163.
19. Zhai, C., et al., *Discovery and design of soft polymeric bio-inspired materials with multiscale simulations and artificial intelligence*. 2020. **8**(31): p. 6562-6587.
20. Liu, Y., et al., *Materials discovery and design using machine learning*. Journal of Materiomics, 2017. **3**(3): p. 159-177.
21. Meng, L., et al., *Machine learning in additive manufacturing: A review*. 2020. **72**(6): p. 2363-2377.

22. Mao, Y., Q. He, and X. Zhao, *Designing complex architected materials with generative adversarial networks*. *Sci Adv*, 2020. **6**(17): p. eaaz4169.
23. Goh, G., S. Sing, and W.J.A.I.R. Yeong, *A review on machine learning in 3D printing: Applications, potential, and challenges*. 2021. **54**(1): p. 63-94.
24. Barthelat, F., *Architected materials in engineering and biology: fabrication, structure, mechanics and performance*. *International Materials Reviews*, 2016. **60**(8): p. 413-430.
25. Ottani, V., et al., *Hierarchical structures in fibrillar collagens*. *Micron*, 2002. **33**(7-8): p. 587-96.
26. Kluge, J.A., et al., *Spider silks and their applications*. *Trends in Biotechnology*, 2008. **26**(5): p. 244-251.
27. Aizenberg, J., et al., *Skeleton of Euplectella sp.: structural hierarchy from the nanoscale to the macroscale*. *Science*, 2005. **309**(5732): p. 275-8.
28. Lenau, T. and M. Barfoed, *Colours and metallic sheen in beetle shells—a biomimetic search for material structuring principles causing light interference*. *Advanced Engineering Materials*, 2008. **10**(4): p. 299-314.
29. Bruet, B.J., et al., *Materials design principles of ancient fish armour*. *Nat Mater*, 2008. **7**(9): p. 748-56.
30. Cribb, B.W., et al., *Structure, composition and properties of naturally occurring non-calcified crustacean cuticle*. *Arthropod Struct Dev*, 2009. **38**(3): p. 173-8.
31. Barthelat, F., et al., *On the mechanics of mother-of-pearl: A key feature in the material hierarchical structure*. *Journal of the Mechanics and Physics of Solids*, 2007. **55**(2): p. 306-337.
32. Barthelat, F. and H. Espinosa, *An experimental investigation of deformation and fracture of nacre—mother of pearl*. *Experimental mechanics*, 2007. **47**(3): p. 311-324.
33. Kasapi, M.A. and J.M. Gosline, *Design complexity and fracture control in the equine hoof wall*. *J Exp Biol*, 1997. **200**(Pt 11): p. 1639-59.
34. Fuller, L.H. and S.W. Donahue, *Material properties of bighorn sheep (Ovis canadensis) horncore bone with implications for energy absorption during impacts*. *J Mech Behav Biomed Mater*, 2021. **114**: p. 104224.
35. Jia, Z., Y. Yu, and L.F. Wang, *Learning from nature: Use material architecture to break the performance tradeoffs*. *Materials & Design*, 2019. **168**: p. 107650.
36. Rhee, H., et al., *A study on the structure and mechanical behavior of the Terrapene carolina carapace: A pathway to design bio-inspired synthetic composites*. *Materials Science & Engineering C-Materials for Biological Applications*, 2009. **29**(8): p. 2333-2339.
37. Naleway, S.E., et al., *Structural Design Elements in Biological Materials: Application to Bioinspiration*. *Adv Mater*, 2015. **27**(37): p. 5455-76.
38. Chen, I.H., et al., *Armadillo armor: mechanical testing and micro-structural evaluation*. *J Mech Behav Biomed Mater*, 2011. **4**(5): p. 713-22.
39. Li, Y., C. Ortiz, and M.C. Boyce, *Bioinspired, mechanical, deterministic fractal model for hierarchical suture joints*. *Phys Rev E Stat Nonlin Soft Matter Phys*, 2012. **85**(3 Pt 1): p. 031901.
40. Porter, M.M., et al., *Highly deformable bones: unusual deformation mechanisms of seahorse armor*. *Acta Biomater*, 2013. **9**(6): p. 6763-70.
41. Yang, W., et al., *Natural flexible dermal armor*. *Adv Mater*, 2013. **25**(1): p. 31-48.

42. Feng, Y., et al., *Impact mechanics of topologically interlocked material assemblies*. International Journal of Impact Engineering, 2015. **75**: p. 140-149.
43. A.V. Dyskin, Y.E., E. Pasternak, H.C. Khor, A.J. Kanel-Belov, *Fracture resistant structures based on topological interlocking with non-planar contacts*. Adv. Eng. Materials & Design, 2003. **5**: p. 116-119.
44. Goodman, R.E. and G.-h. Shi, *Block theory and its application to rock engineering*. 1985.
45. Dyskin, A.V., et al., *Toughening by fragmentation—how topology helps*. 2001. **3**(11): p. 885-888.
46. Khandelwal, S., et al., *Adaptive mechanical properties of topologically interlocking material systems*. Smart Materials and Structures, 2015. **24**(4).
47. Khandelwal, S., et al., *Transverse loading of cellular topologically interlocked materials*. International Journal of Solids and Structures, 2012. **49**(18): p. 2394-2403.
48. Mather, A., R. Cipra, and T.J.I.J.o.S.I. Siegmund, *Structural integrity during remanufacture of a topologically interlocked material*. 2012.
49. Dyskin, A.V., et al., *A new concept in design of materials and structures: Assemblies of interlocked tetrahedron-shaped elements*. 2001. **44**(12): p. 2689-2694.
50. Mirkhalaf, M., et al., *Toughness by segmentation: Fabrication, testing and micromechanics of architected ceramic panels for impact applications*. International Journal of Solids and Structures, 2019. **158**: p. 52-65.
51. Dyskin, A.V., et al., *The principle of topological interlocking in extraterrestrial construction*. Acta Astronautica, 2005. **57**(1): p. 10-21.
52. Krause, T., et al., *Mechanical properties of topologically interlocked structures with elements produced by freeze gelation of ceramic slurries*. 2012. **14**(5): p. 335-341.
53. Autruffe, A., et al., *Indentation Behaviour of Interlocked Structures Made of Ice: Influence of the Friction Coefficient*. Advanced Engineering Materials, 2007. **9**(8): p. 664-666.
54. Mirkhalaf, M., T. Zhou, and F. Barthelat, *Simultaneous improvements of strength and toughness in topologically interlocked ceramics*. Proc Natl Acad Sci U S A, 2018. **115**(37): p. 9128-9133.
55. Yin, Z., F. Hannard, and F. Barthelat, *Impact-resistant nacre-like transparent materials*. Science, 2019. **364**(6447): p. 1260-1263.
56. Carlesso, M., et al., *Improvement of sound absorption and flexural compliance of porous alumina-mullite ceramics by engineering the microstructure and segmentation into topologically interlocked blocks*. Journal of the European Ceramic Society, 2013. **33**(13-14): p. 2549-2558.
57. Dugué, M., et al., *Indentation of interlocked assemblies: 3D discrete simulations and experiments*. Computational Materials Science, 2013. **79**: p. 591-598.
58. Khandelwal, S., et al., *Scaling of the elastic behavior of two-dimensional topologically interlocked materials under transverse loading*. 2014. **81**(3).
59. Schaare, S., et al., *Point loading of assemblies of interlocked cube-shaped elements*. International Journal of Engineering Science, 2008. **46**(12): p. 1228-1238.
60. Bishop, C.M., *Pattern recognition and machine learning*. 2006: springer.
61. Chua, L.O., L.J.I.T.o.c. Yang, and systems, *Cellular neural networks: Theory*. 1988. **35**(10): p. 1257-1272.
62. McCulloch, W.S. and W.J.T.b.o.m.b. Pitts, *A logical calculus of the ideas immanent in nervous activity*. 1943. **5**(4): p. 115-133.

63. Widrow, B. and M.E. Hoff, *Adaptive switching circuits*. 1960, Stanford Univ Ca Stanford Electronics Labs.
64. Rosenblatt, F., *Principles of neurodynamics: Perceptions and the theory of brain mechanisms*. 1962.
65. McClelland, J.L., D.E. Rumelhart, and P.R.G.J.E.i.t.M.o. Cognition, *Parallel distributed processing*. 1986. **2**: p. 216-271.
66. Pal, S.K. and S. Mitra, *Multilayer perceptron, fuzzy sets, classification*. 1992.
67. Ruck, D.W., et al., *The multilayer perceptron as an approximation to a Bayes optimal discriminant function*. 1990. **1**(4): p. 296-298.
68. Bishop, C.M., *Neural networks for pattern recognition*. 1995: Oxford university press.
69. Ben-Hur, A., et al., *Support vector clustering*. 2001. **2**(Dec): p. 125-137.
70. Salcedo-Sanz, S., et al., *Support vector machines in engineering: an overview*. 2014. **4**(3): p. 234-267.
71. Wang, Y. and I.H. Witten, *Induction of model trees for predicting continuous classes*. 1996.
72. Friedman, J.H.J.A.o.s., *Greedy function approximation: a gradient boosting machine*. 2001: p. 1189-1232.
73. Pollard, A., et al., *Whither turbulence and big data in the 21st century?* 2016: Springer.
74. Brunton, S.L., B.R. Noack, and P. Koumoutsakos, *Machine Learning for Fluid Mechanics*. Annual Review of Fluid Mechanics, 2020. **52**(1): p. 477-508.
75. Wuest, T., et al., *Machine learning in manufacturing: advantages, challenges, and applications*. Production & Manufacturing Research, 2016. **4**(1): p. 23-45.
76. Monostori, L., et al., *Machine learning approaches to manufacturing*. 1996. **45**(2): p. 675-712.
77. Wagstaff, K.J.a.p.a., *Machine learning that matters*. 2012.
78. García-Ordás, M., *Wear characterization of the cutting tool in milling processes using shape and texture descriptors*. 2017, Universidad de León.
79. Cho, S., et al., *Tool breakage detection using support vector machine learning in a milling process*. 2005. **45**(3): p. 241-249.
80. Wu, D., et al., *A comparative study on machine learning algorithms for smart manufacturing: tool wear prediction using random forests*. 2017. **139**(7).
81. Jurkovic, Z., et al., *A comparison of machine learning methods for cutting parameters prediction in high speed turning process*. 2018. **29**(8): p. 1683-1693.
82. Čojbašić, Ž., et al., *Surface roughness prediction by extreme learning machine constructed with abrasive water jet*. 2016. **43**: p. 86-92.
83. Deris, A.M., A.M. Zain, and R.J.M. Sallehuddin, *Hybrid GR-SVM for prediction of surface roughness in abrasive water jet machining*. 2013. **48**(8): p. 1937-1945.
84. Rakshit, R. and A.K.J.P.E. Das, *A review on cutting of industrial ceramic materials*. 2019. **59**: p. 90-109.
85. Jianxin, D. and L.J.C.I. Taichiu, *Surface integrity in electro-discharge machining, ultrasonic machining, and diamond saw cutting of ceramic composites*. 2000. **26**(8): p. 825-830.
86. Li, K. and T.W.J.J.o.M.P.T. Liao, *Surface/subsurface damage and the fracture strength of ground ceramics*. 1996. **57**(3-4): p. 207-220.
87. Fenoughty, K., A. Jawaid, and I.J.J.o.m.p.t. Pashby, *Machining of advanced engineering materials using traditional and laser techniques*. 1994. **42**(4): p. 391-400.

88. Samant, A.N. and N.B.J.J.o.t.E.c.s. Dahotre, *Laser machining of structural ceramics—A review*. 2009. **29**(6): p. 969-993.
89. Pham, D., et al., *Laser milling of ceramic components*. 2007. **47**(3-4): p. 618-626.
90. Viskup, R., *High Energy and Short Pulse Lasers*. 2016: BoD—Books on Demand.
91. Beausoleil, C., et al., *Deep and high precision cutting of alumina ceramics by picosecond laser*. 2020.
92. Ackerl, N. and K.J.J.o.L.M.N. Wegener, *Ablation characteristics of alumina and zirconia ceramics on ultra-short pulsed laser machining*. 2019. **14**(2): p. 168-172.
93. Umer, U., M.K. Mohammed, and A.J.M. Al-Ahmari, *Multi-response optimization of machining parameters in micro milling of alumina ceramics using Nd: YAG laser*. 2017. **95**: p. 181-192.
94. Esmail, I., et al., *Engineered net shaping of alumina ceramics using picosecond laser*. 2021. **135**: p. 106669.
95. Dhara, S.K., A.S. Kuar, and S. Mitra, *An artificial neural network approach on parametric optimization of laser micro-machining of die-steel*. The International Journal of Advanced Manufacturing Technology, 2007. **39**(1-2): p. 39-46.
96. Kumar, A., M.C.J.O. Gupta, and L.i. Engineering, *Laser machining of micro-notches for fatigue life*. 2010. **48**(6): p. 690-697.
97. Karazi, S., et al., *Comparison of ANN and DoE for the prediction of laser-machined micro-channel dimensions*. 2009. **47**(9): p. 956-964.
98. Desai, C.K. and A.J.T.I.J.o.A.M.T. Shaikh, *Prediction of depth of cut for single-pass laser micro-milling process using semi-analytical, ANN and GP approaches*. 2012. **60**(9-12): p. 865-882.
99. Bustillo, A. and M.J.J.o.I.M. Correa, *Using artificial intelligence to predict surface roughness in deep drilling of steel components*. 2012. **23**(5): p. 1893-1902.
100. Hosmer, D.W., et al., *A comparison of goodness-of-fit tests for the logistic regression model*. Stat Med, 1997. **16**(9): p. 965-80.
101. Li, Y.Z. and Y. Yuan, *Convergence Analysis of Two-layer Neural Networks with ReLU Activation*. Advances in Neural Information Processing Systems 30 (Nips 2017), 2017. **30**: p. 597-607.
102. Eckle, K. and J. Schmidt-Hieber, *A comparison of deep networks with ReLU activation function and linear spline-type methods*. Neural Netw, 2019. **110**: p. 232-242.
103. Beausoleil, C., et al., *Deep and high precision cutting of alumina ceramics by picosecond laser*. Ceramics International, 2020.
104. Ward, L., et al., *A general-purpose machine learning framework for predicting properties of inorganic materials*. 2016. **2**(1): p. 1-7.
105. Goh, G.B., N.O. Hodas, and A. Vishnu, *Deep learning for computational chemistry*. J Comput Chem, 2017. **38**(16): p. 1291-1307.
106. Paliana, G., et al., *Accelerating materials property predictions using machine learning*. 2013. **3**(1): p. 1-6.
107. Zhang, Z. and K. Friedrich, *Artificial neural networks applied to polymer composites: a review*. Composites Science and Technology, 2003. **63**(14): p. 2029-2044.
108. Bisagni, C. and L. Lanzi, *Post-buckling optimisation of composite stiffened panels using neural networks*. Composite Structures, 2002. **58**(2): p. 237-247.
109. Guo, K., et al., *Artificial intelligence and machine learning in design of mechanical materials*. 2021.

110. Alakent, B., S.J.I. Soyer-Uzun, and E.C. Research, *Implementation of statistical learning methods to develop guidelines for the design of PLA-based composites with high tensile strength values*. 2019. **58**(8): p. 3478-3489.
111. Chen, C.T., G.X.J.A.T. Gu, and Simulations, *Effect of constituent materials on composite performance: exploring design strategies via machine learning*. 2019. **2**(6): p. 1900056.
112. Gu, G.X., C.T. Chen, and M.J. Buehler, *De novo composite design based on machine learning algorithm*. Extreme Mechanics Letters, 2018. **18**: p. 19-28.
113. Qi, C.C., A. Fourie, and Q.S. Chen, *Neural network and particle swarm optimization for predicting the unconfined compressive strength of cemented paste backfill*. Construction and Building Materials, 2018. **159**: p. 473-478.
114. Tiryaki, S. and A. Aydin, *An artificial neural network model for predicting compression strength of heat treated woods and comparison with a multiple linear regression model*. Construction and Building Materials, 2014. **62**: p. 102-108.
115. Yang, Z.J., et al., *Deep learning approaches for mining structure-property linkages in high contrast composites from simulation datasets*. Computational Materials Science, 2018. **151**: p. 278-287.
116. Yang, Z.J., et al., *Establishing structure-property localization linkages for elastic deformation of three-dimensional high contrast composites using deep learning approaches*. Acta Materialia, 2019. **166**: p. 335-345.
117. King, T.G., et al., *Piezoelectric Ceramic Actuators - a Review of Machinery Applications*. Precision Engineering-Journal of the American Society for Precision Engineering, 1990. **12**(3): p. 131-137.
118. Schmidt, R.P., *Aircraft thermal protection system*. 1996, Google Patents.
119. Kalita, S.J., A. Bhardwaj, and H.A. Bhatt, *Nanocrystalline calcium phosphate ceramics in biomedical engineering*. Materials Science & Engineering C-Biomimetic and Supramolecular Systems, 2007. **27**(3): p. 441-449.
120. Bal, B.S. and M.N. Rahaman, *Orthopedic applications of silicon nitride ceramics*. Acta Biomater, 2012. **8**(8): p. 2889-98.
121. Shackelford, J.F., *Bioceramics: Applications of ceramic and glass materials in medicine*. 1999: Trans Tech Publications Switzerland.
122. Evans, A.G., *Perspective on the development of high-toughness ceramics*. Journal of the American Ceramic society, 1990. **73**(2): p. 187-206.
123. Justin, J. and A. Jankowiak, *Ultra High Temperature Ceramics: Densification, Properties and Thermal Stability*. 2011.
124. Sarvestani, H.Y., et al., *Multilayered architected ceramic panels with weak interfaces: energy absorption and multi-hit capabilities*. Materials & Design, 2019. **167**: p. 107627.
125. Sarvestani, H.Y., et al., *Architected ceramics with tunable toughness and stiffness*. Extreme Mechanics Letters, 2020. **39**: p. 100844.
126. Liu, K. and L. Jiang, *Multifunctional integration: from biological to bio-inspired materials*. Acs Nano, 2011. **5**(9): p. 6786-6790.
127. Meyers, M.A., et al., *Structural biological composites: An overview*. Jom, 2006. **58**(7): p. 35-41.
128. Zhang, C., D.A. Mcadams, and J.C. Grunlan, *Nano/Micro-Manufacturing of Bioinspired Materials: a Review of Methods to Mimic Natural Structures*. Advanced Materials, 2016. **28**(30): p. 6292-6321.

129. Cheng, Q., L. Jiang, and Z. Tang, *Bioinspired layered materials with superior mechanical performance*. *Acc Chem Res*, 2014. **47**(4): p. 1256-66.
130. Barthelat, F., *Architected materials in engineering and biology: fabrication, structure, mechanics and performance*. *International Materials Reviews*, 2015. **60**(8): p. 413-430.
131. Fleck, N.A., V.S. Deshpande, and M.F. Ashby, *Micro-architected materials: past, present and future*. *Proceedings of the Royal Society a-Mathematical Physical and Engineering Sciences*, 2010. **466**(2121): p. 2495-2516.
132. Rudykh, S., C. Ortiz, and M.C. Boyce, *Flexibility and protection by design: imbricated hybrid microstructures of bio-inspired armor*. *Soft Matter*, 2015. **11**(13): p. 2547-2554.
133. Djumas, L., et al., *Deformation mechanics of non-planar topologically interlocked assemblies with structural hierarchy and varying geometry*. *Scientific reports*, 2017. **7**(1): p. 1-11.
134. Slesarenko, V., N. Kazarinov, and S. Rudykh, *Distinct failure modes in bio-inspired 3D-printed staggered composites under non-aligned loadings*. *Smart Materials and Structures*, 2017. **26**(3): p. 035053.
135. Flores-Johnson, E.A., et al., *Numerical investigation of the impact behaviour of bioinspired nacre-like aluminium composite plates*. *Composites Science and Technology*, 2014. **96**: p. 13-22.
136. Grunenfelder, L.K., et al., *Bio-inspired impact-resistant composites*. *Acta Biomater*, 2014. **10**(9): p. 3997-4008.
137. Gu, G.X., M. Takaffoli, and M.J. Buehler, *Hierarchically Enhanced Impact Resistance of Bioinspired Composites*. *Adv Mater*, 2017. **29**(28).
138. Dyskin, A.V., et al., *Fracture resistant structures based on topological interlocking with non-planar contacts*. *Advanced Engineering Materials*, 2003. **5**(3): p. 116-119.
139. Kourou, K., et al., *Machine learning applications in cancer prognosis and prediction*. *Comput Struct Biotechnol J*, 2015. **13**: p. 8-17.
140. Vamathevan, J., et al., *Applications of machine learning in drug discovery and development*. *Nat Rev Drug Discov*, 2019. **18**(6): p. 463-477.
141. Erickson, B.J., et al., *Machine Learning for Medical Imaging(1)*. *Radiographics*, 2017. **37**(2): p. 505-515.
142. Gu, G.X., et al., *Bioinspired hierarchical composite design using machine learning: simulation, additive manufacturing, and experiment*. *Materials Horizons*, 2018. **5**(5): p. 939-945.
143. Pilania, G., et al., *Accelerating materials property predictions using machine learning*. *Scientific Reports*, 2013. **3**(1): p. 1-6.
144. Liu, R., et al., *A predictive machine learning approach for microstructure optimization and materials design*. *Sci Rep*, 2015. **5**(1): p. 11551.
145. Budynas, R.G. and J.K. Nisbett, *Shigley's mechanical engineering design*. Vol. 8. 2008: McGraw-Hill New York.
146. Hetnarski, R.B., M.R. Eslami, and G. Gladwell, *Thermal stresses: advanced theory and applications*. Vol. 158. 2009: Springer.
147. Esmail, I., et al., *Engineered net shaping of alumina ceramics using picosecond laser*. *Optics & Laser Technology*, 2021. **135**.